Geomorphology 123 (2010) 211–231

Contents lists available at ScienceDirect

Geomorphology

journal homepage: www.elsevier.com/locate/geomorph

Thrust-fold activity at the mountain front of the Northern Apennines (Italy) from quantitative landscape analysis

Alessio Ponza [a,*], Frank J. Pazzaglia [b], Vincenzo Picotti [a]

[a] Università di Bologna, Dipartimento di Scienze del la Terra e Geologico Ambientali, Via Zamboni 67, 40126 Bologna, Italy
[b] Department of Earth and Environmental Science, Lehigh University, 31 Williams, Bethlehem, PA 18015, USA

ARTICLE INFO

Article history:
Received 18 November 2009
Received in revised form 22 May 2010
Accepted 1 June 2010
Available online 18 June 2010

Keywords:
Active folding
Topography
Tectonic geomorphology
Long profile modeling
Foothills of the northern Apennines

ABSTRACT

We document the active tectonics of growing anticlines embedded in the northern Apennine mountain front using a quantitative analysis of the topography. These structures appear to be growing at rates of 0.1–0.3 mm/year, more slowly than the long-term general rate of emergence of the Apennines from the Po plain. Our analysis is dedicated to extract the signal of this tectonic activity, recording it primarily by the channel steepness (k_{sn}) of streams traversing the mountain front and by swath profiles and relief of the topography. Topographic swath profiles and k_{sn} are consistent with field stratigraphic, structural mapping and seismic reflection profile relationships. In general, the spatial distribution of k_{sn} values of small channels (with upstream drainage area <20 km^2) appears to coincide with fold uplift and deformation, being the maxima located at the fold axes, towards the foreland or along strike as the tilting of a growing fold propagates frontally or laterally.

Quantitatively, we use local development of relief as a proxy for rock uplift (measured as river incision) across the mountain front and anticlines to test the expected linear scaling between rock-uplift rates (relief) and k_{sn}. In this low rock-uplift setting (0.1–0.3 mm/year), this predicted scaling relationship is not supported by k_{sn} and topographic data, suggesting a condition of transient response of fluvial incision that generates the relief to the tectonic forcing, where k_{sn} and relief have not achieved steady-state values. However, a weak linear scaling between rock uplift and k_{sn} may hold for the local highest uplift settings where over 40 m of relief have been generated, thus establishing a lower threshold for where the channel steepness approach may be valid.

In this slowly deforming landscape assuming a state of transient response of fluvial incision to tectonic forcing, the high k_{sn} values can be explained as places where the channels are being actively deformed by tectonics, but have not yet fully responded by incising and generating relief. Therefore, in the absence of relief generation, the spatial distribution of k_{sn} maximum values for small streams can hold for rock uplift and work as a model for indicating locations of strongest anticlinal growth.

Collectively, the correspondence among the stratigraphic markers used to define the structures, topography and relief as quantified in the swath profiles, and the k_{sn} values that indicate active channel adjustments to tectonic forcing support the evidence of continued shortening across the European–Adria plate boundary and the contemporary slow growth of the structures embedded in the emergent Apennines mountain front.

1. Introduction

The northern Apennines and Po foreland (Fig. 1) are usually described as a thin skinned Tertiary fold and thrust belt (e.g. Bally et al., 1986; Hill and Hayward, 1988). Since the Middle Pleistocene, deformation in the northern Apennines has stepped back from the deformation front and appears to be concentrated in building a mountain front that defines the southern boundary of the Po basin (Picotti and Pazzaglia, 2008), defined by deformation of fluvial and marginal marine deposits preserved there. In this paper, we present topographic, stratigraphic, and geomorphic evidence for active tectonic deformation consistent in scale and style with the pre-middle Pleistocene fold- and thrust-belt deformation. This deformation contrasts with larger scale processes that are building the mountain front, but also reaffirms that the northern Apennines and Po plain define a belt of active compression in the foreland (Elter et al., 1975).

We focus on the analysis of fluvial channels, Quaternary deposits, and swath topographic profiles in two zones located ~40 and ~80 km west of the Reno valley, the Castelvetro–Vignola foothills and the Ghiardo plateau near San Polo d'Enza (Figs. 2 and 3, respectively). We

* Corresponding author. Tel.: +39 051 2094546; fax: +39 051 2094522.
E-mail addresses: alessio.ponza@unibo.it (A. Ponza), fjp3@lehigh.edu (F.J. Pazzaglia), vincenzo.picotti@unibo.it (V. Picotti).

0169-555X/$ – see front matter © 2010 Elsevier B.V. All rights reserved.
doi:10.1016/j.geomorph.2010.06.008

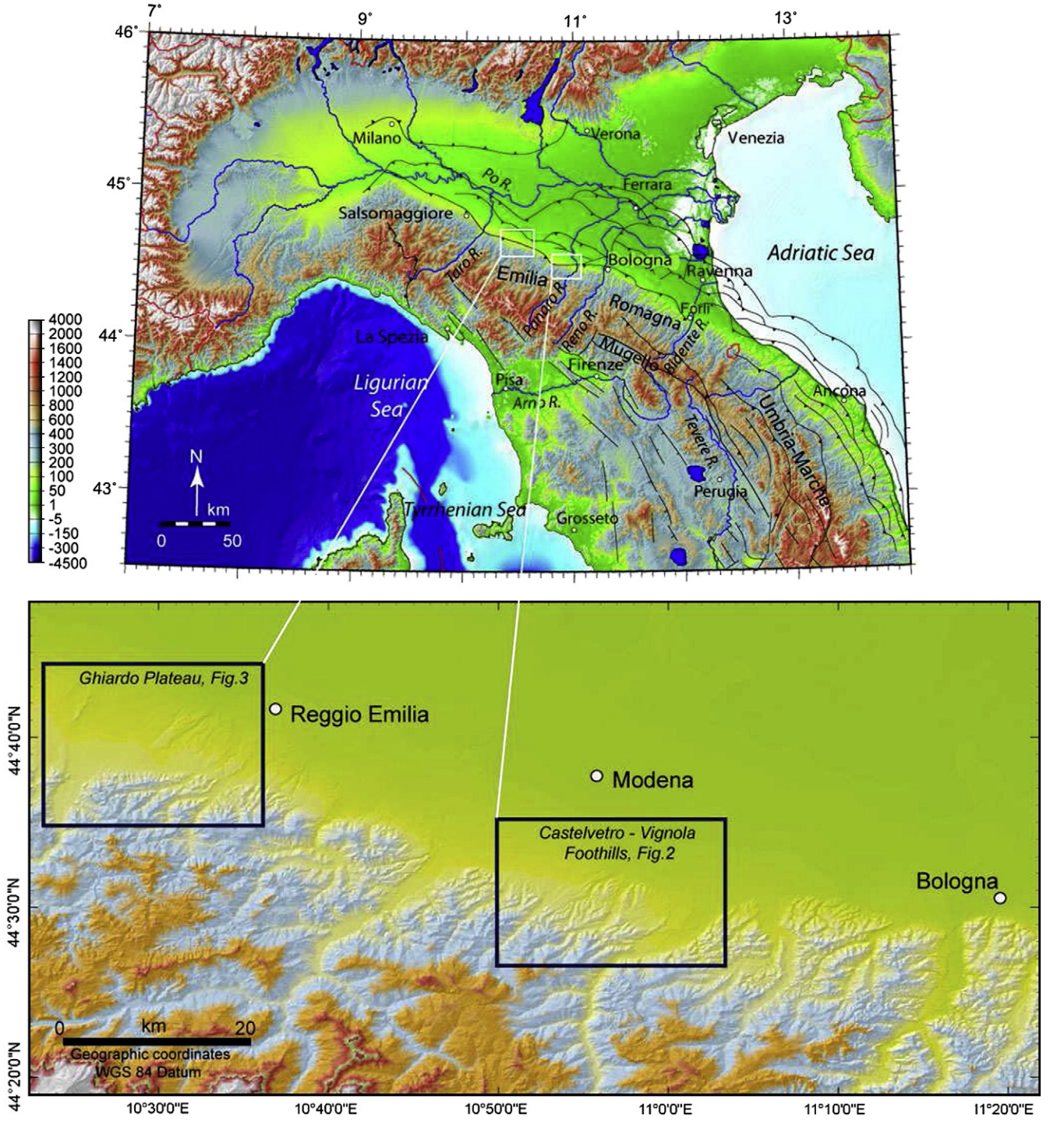

Fig. 1. Topography of the northern Apennines derived from 90-m SRTM digital elevation model. Key regions and drainage systems are labeled. Colored boxes localize the studied areas in the foothills zone.

investigate these areas because earlier geomorphic and structural geology studies argued for active tectonic deformation and topographic growth of low hills on the margin of the Po plain (Cremaschi and Papani, 1975; Gasperi et al., 1999). Additionally, Late Middle Pleistocene to Holocene rates of rock uplift at the mountain front have been recently interpreted to range from 0.3 to 2.2 mm/year for three parts of the northern Apennines, relying primarily on fluvial incision through deformed geomorphic markers from NW to SE, respectively, the Salsomaggiore anticline (Wilson et al., 2009), the Reno valley at Bologna (Picotti and Pazzaglia, 2008), and the Bidente River at Forlì (Wegmann and Pazzaglia, 2009) (see Fig. 1).

Our analysis is dedicated to extract the active tectonic signal, recorded primarily by the channel steepness of streams traversing the mountain front. The general correspondence of modeled stream steepness to rock uplift is complicated by variations in rock type, bedload conditions, stream widths, and channel transients. Nevertheless, in numerous studies (e.g. Snyder et al., 2000; Kirby and Whipple, 2001; Wobus et al., 2006), variations of the steepness

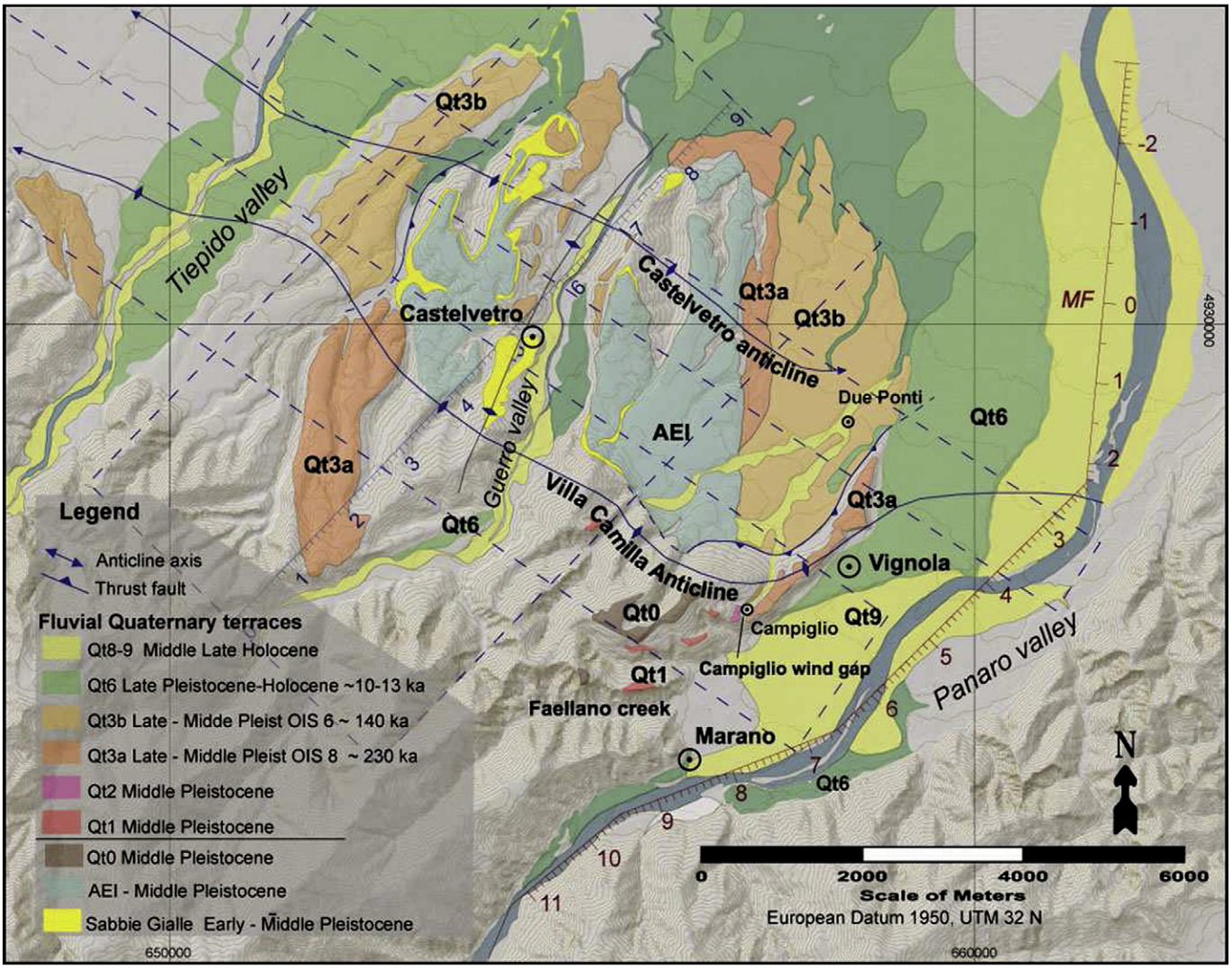

Fig. 2. Geologic map of the Castelvetro–Vignola area modified from Gasperi et al. (1999), Carta Geologica d'Italia, scale 1:50,000, foglio Sassuolo and partially compiled from Regione Emilia–Romagna. Dashed blue boxes show the surfaces of swath profiles in Figs. 6, 7. Quaternary fluvial terraces chronostratigraphy follows Picotti and Pazzaglia (2008) and Wegmann and Pazzaglia (2009). Qt holds for quaternary terrace continental deposit, while numbering increases starting from the oldest to the younger deposit.

indexes along a stream long profile have been demonstrated to co-vary with rock uplift, revealing robust and important qualitative results. The highest steepness values tend to linearly correspond to the regions with highest rock uplift and exhumation rates.

Previous studies explored regions where the tectonic signal is strongly identifiable and field areas can be neatly divided into high and low-uplift zones: here the tectonics can be (i) independently determined, (ii) it is variable at a wide regional scale and, (iii) exhibits consistent differences, of at least an order of magnitude, between high and low Pleistocene and Holocene rock-uplift rates. These magnitudes of the tectonic forcing range from 4 mm/year to 0.5 mm/year in the Mendocino triple junction region of northern California (Merritts and Bull, 1989; Merritts, 1996; Snyder et al., 2000; Kirby and Whipple, 2001); from 2–3 mm/year to 0.5 mm/year in the San Gabriel Mountains, California (Blythe et al., 2000; Wobus et al., 2006); from 17 mm/year to 0 mm/year in the Siwalik hills, central Nepal (Wobus et al., 2006).

The Apennines mountain front study case appears particularly suitable, in that lithologic variations are minor, with the whole foothills range being underlain by relatively soft Plio-Pleistocene mudstone, sandstone, and conglomerate. Similarly, no significant climatic gradients exist and the history and influence over the Late Pleistocene to Holocene denudation is fairly well known (e.g., Wegmann and Pazzaglia, 2009). In such a setting, we intend to study small structures rising along the northern Apennines mountain front, and uplifting at low rates of 0.1–0.3 mm/year (according to Ponza, 2010, Ph.D. dissertation). As a result, our approach provides a test for establishing the lower threshold signal of channel response to low tectonic activity.

2. Geologic setting

2.1. The Northern Apennines

The northern Apennines are a fold and thrust belt developed as the pro-wedge of the subducting Adria plate since the Oligocene. They are a well-recognized example of a plate boundary characterized by a retreating upper plate and lower-plate slab rollback (*sensu* Royden, 1993), for their coeval character of compression at the front and extension at the hinterland (Elter et al., 1975). The present day

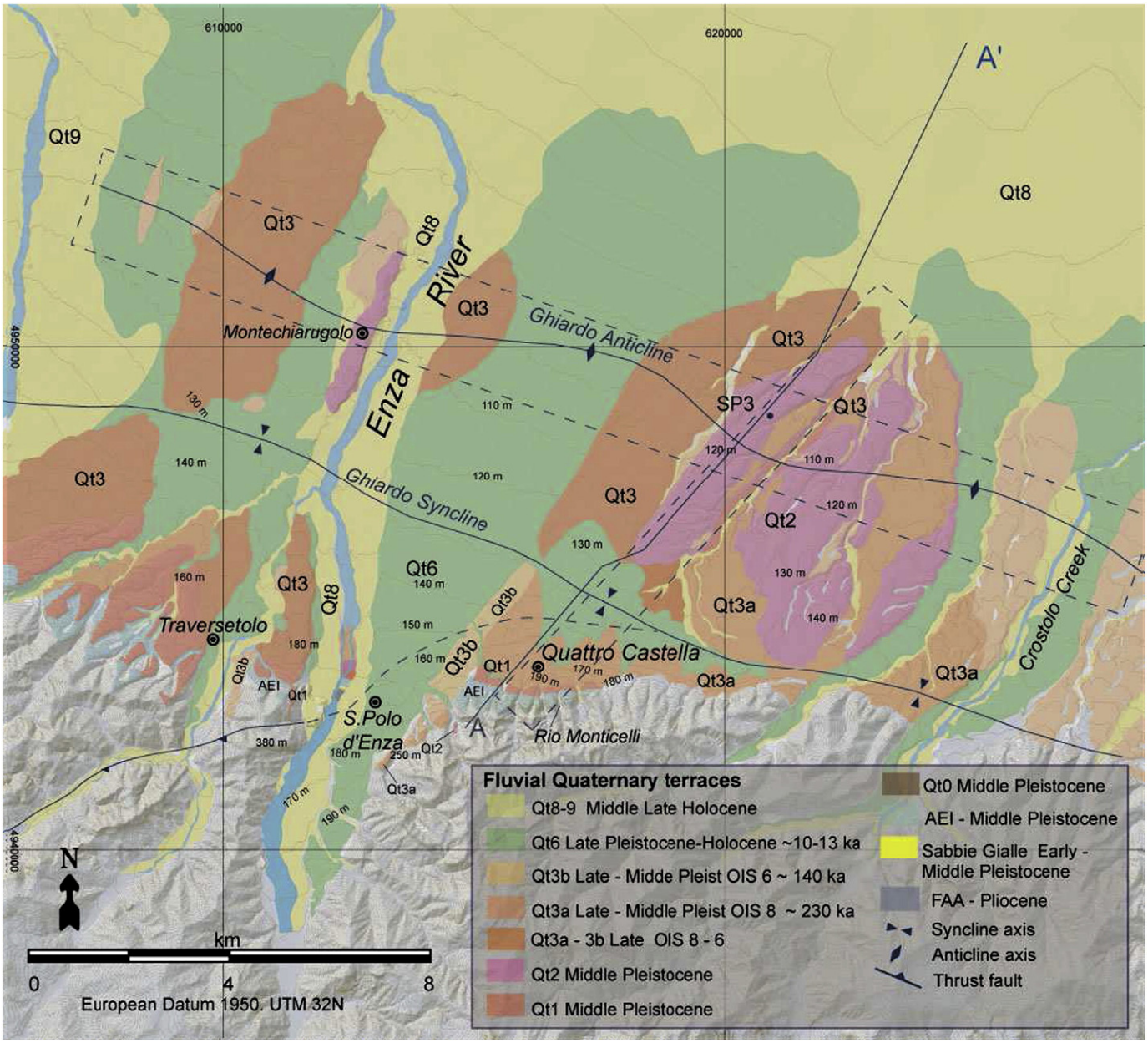

Fig. 3. Geologic map of the Ghiardo area modified from Carnicelli et al. (2003) and partially compiled from Regione Emilia–Romagna. Quaternary fluvial terraces chronostratigraphy in accordance with Picotti and Pazzaglia (2008) and Wegmann and Pazzaglia (2009). Dashed blue boxes show the surfaces of the swath profiles of Fig. 8, and AA′ is the trace of the geological section of Fig. 4. Geologic structures traces are adjusted on the base of well stratigraphy and seismic lines.

mountain range is characterized by rapid Pliocene and Pleistocene uplift and exhumation (Balestrieri et al., 2003; Bartolini, 2003). The northern Apennines mountain front and its adjoining foothills are riddled with geologic and geomorphic evidence of active tectonics, such as growing folds and faults that collectively represent the near-surface structural response of ongoing Adria–Europe convergence (see Picotti and Pazzaglia, 2008, with references).

The main mountain front of the northern Apennines is commonly viewed as some version of a continuous thrust structure (also known as Pede-Apenninic Thrust Front PTF; Boccaletti et al., 1985; see Fig. 1) that offsets Quaternary deposits and locally may be emergent as an out-of-sequence thrust rooted deep in the wedge (e.g. Lavecchia et al., 2003, 2004; Boccaletti et al., 2004; Picotti and Pazzaglia, 2008). In contrast, the buried front of the northern Apennines, i.e., the most external thrust, is sometimes viewed as the true active front of the northern Apennines (Scrocca, 2006). However, this interpretation can explain neither the growth during the Quaternary of the main geomorphic feature, i.e., the mountain front, nor the absence of relief in correspondence of the external thrust, that, moreover, appears sealed in subsurface by the Pleistocene deposits.

Near Bologna the PTF or its attendant splays do not appear to be emergent. Here, the PTF is a deep, steep, blind structure associated with the frontal limb of an antiform that defines the mountain front (Picotti and Pazzaglia, 2008). However, locally west of Bologna (Fig. 1) in the Emilia foothills and adjacent to the Po plain, shallow splays of the PTF remain active in the Miocene–Pliocene thrust belt (e.g., Scrocca et al., 2007). In this area, the geometry of the Quaternary structures is rather complex, in places characterized by dome-and-

swell features, suggesting interaction of different shortening directions (Gasperi et al., 1999; Picotti et al., 2007).

2.2. Castelvetro–Vignola hill and Ghiardo plateau

The southern flank of the Po plain in the vicinity of Castelvetro and the Ghiardo plateau is corrugated into a series of low, elongated hills and valleys that have long been associated with actively growing folds (Cremaschi and Papani, 1975; Gasperi et al., 1999; Carnicelli et al., 2003; Figs. 2–4). The Castelvetro fold is ~4 km in amplitude, ~15 km in strike length, and is bound to the east by the Panaro River and to the west by the Tiepido River (Fig. 2). The Castelvetro folds show evidence of the interaction of two deformation trends: a WNW (Apenninic) and a NE (anti-Apenninic) trend, with a final dome-and-swell geometry. The limbs of the fold are formed by Plio-Pleistocene deposits and involve Pliocene to Lower Pleistocene mudstone (Argille Azzurre Fm), with local coarse interbeds (Gasperi et al., 1999; Amorosi et al., 1998), middle Pleistocene beach deposits (Sabbie Gialle Fm), and two units of continental deposits: respectively the Lower Emiliano–Romagnolo Synthem (AEI), consisting of coastal plain facies and the Upper Emiliano–Romagnolo Synthem (AES), formed by alluvial plain facies (Gasperi et al., 1999) with growth geometries. The youngest deposits involved in the folding are late middle Pleistocene alluvial units, called AES7/7a in Gasperi et al. (1999) and mapped in this paper (Figs. 2 and 3) as Qt3, following the chronostratigraphy proposed by Picotti and Pazzaglia (2008) and Wegmann and Pazzaglia (2009). The flexure of Villa Camilla is an asimmetric anticline NE oriented that passes near Vignola to a NW trend (Fig. 2). Along the fold hinge, near Campiglio, the topography shows a wind gap carved into the bedrock and dissecting the overlaying Quaternary deposits Qt3 on both sides of the small Campiglio valley. The wind gap is uplifted 45 meters above the terrace immediately lower in the Panaro valley: this alluvial deposits have been recognized as Qt6 in the chronostratigraphy of the Reno valley in Picotti and Pazzaglia (2008) (Unità di Vignola AES7b, following the subdivision of Emilia–Romagna region). Late Pleistocene alluvial terraces are not preserved toward northwest, downstream of the Campiglio wind gap valley.

Farther to the west and between Quattro Castella and Traversetolo, the Enza River carves a valley through Quaternary sediments of the Ghiardo plateau (Fig. 3), an E–W-elongated hill that lies several kilometers north of the mountain front. This latter, south of the Ghiardo plateau, is defined by flatirons striking the topography and underlain by Middle Pleistocene conglomerates. These flatirons led Bernini and Papani (1987) and Boccaletti et al. (2004) to argue for emergence of the PTF, but subsequent map and seismic data show no evidence of such a structure. On the contrary, the Ghiardo plateau is the more likely surface expression of actively growing folds cored by a shallow blind or emergent fault (Figs. 3 and 4). Here, a syncline is infilled by fine-grained upper Pleistocene–Holocene deposits corresponding to the Qt6 chronostratigraphic units of Picotti and Pazzaglia (2008). The top of the plateau is dissected by small N–S

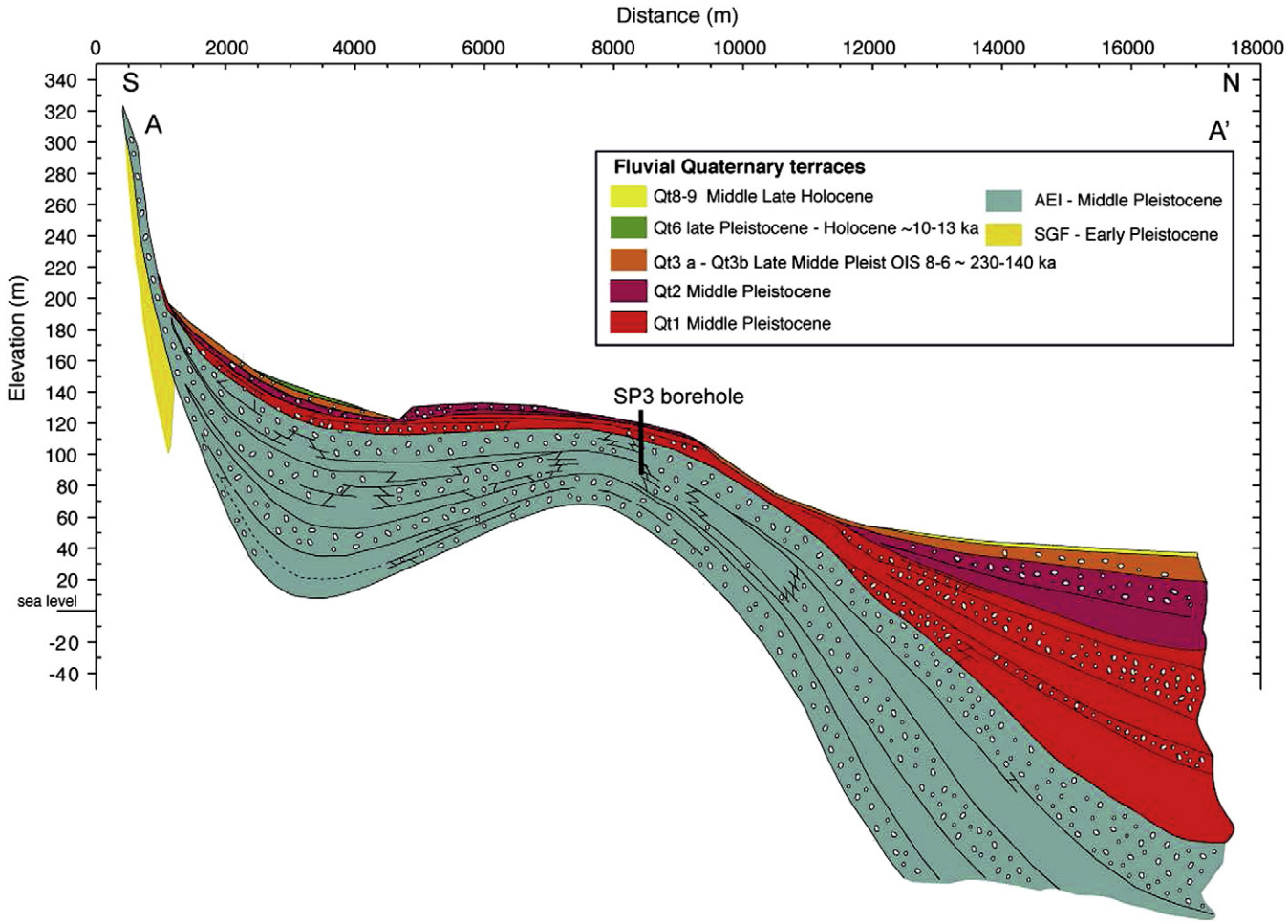

Fig. 4. Geological section across the Ghiardo plateau, modified from Carnicelli et al. (2003): Pleistocene terrace deposits chronostratigraphy is in accordance with Picotti and Pazzaglia (2008) and Wegmann and Pazzaglia (2009).

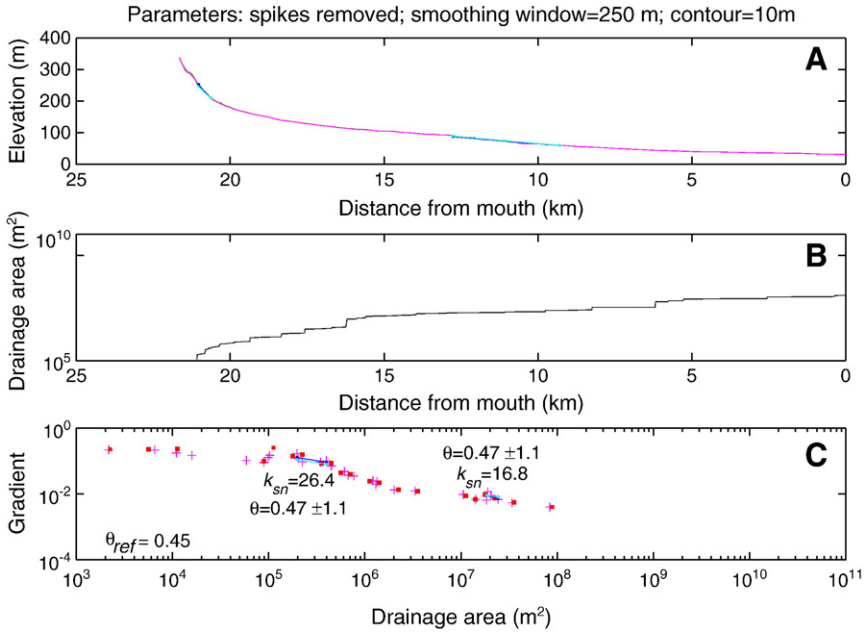

Fig. 5. Channel 13 plot as it results after running the Whipple et al. (2007) tool. Long profile (A), drainage area vs. distance from mouth (B), and log slope vs. log area (C). (A) Raw elevations are in green, smoothed in pink. The dark blue lines are the profiles predicted by the regressed channel concavity; the cyan lines are for the specified reference concavity, θ_{ref}. (C) k_{sn} values extracted from channel reaches: slope of log S vs. log A scaling is the concavity index, where blue and cyan colors show the regressed and reference concavities respectively; y-intercept is the steepness index k_{sn}; red squares are log-bin averages of the slope–area data.

valleys cutting middle to upper Pleistocene continental deposits corresponding to Qt3/Qt2 uplifted above the Holocene plain of the Enza River (Cremaschi and Papani, 1975).

3. Methods

3.1. Lithostratigraphy and uplift rates

The available literature allow us to correlate middle to late Pleistocene marginal marine and continental deposits over a large stretch of the mountain front of the northern Apennines, from the west near Salsomaggiore (Wilson et al., 2009) to Bologna (Picotti and Pazzaglia, 2008) and Forlì area (Wegmann and Pazzaglia, 2009). This correlation is corroborated by the pedological study of Eppes et al. (2008) that defined a soil chronosequence, calibrated with the radiocarbon ages. It is therefore possible to associate, with a good degree of confidence, lithological and pedological observations on alluvial terraces to a well-defined time interval, even in the absence of direct dating. Starting from this frame, in this study we mapped terraces on the chosen areas and we correlate them into chronostratigraphic units.

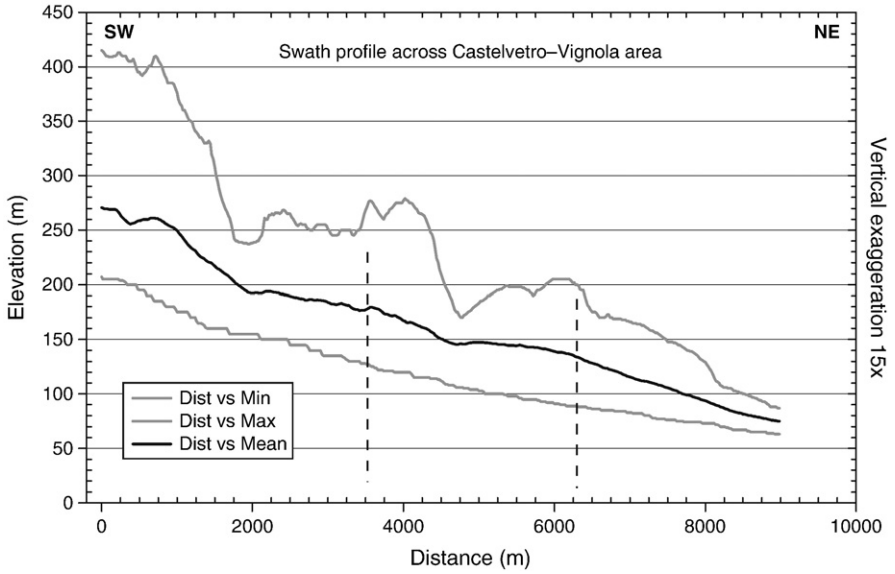

Fig. 6. Swath profile of topography perpendicular to anticlinal hinge of the Castelvetro and the Villa Camilla anticline, vertical exaggeration 15×. Maximum (shaded line), minimum (shaded line), and mean (black line) elevations extracted from a 5-km-wide and 9-km-long swath (location and kilometric profile are shown in the blue dashed box A in Fig. 2). Vertical dashed lines correspond to locations of the anticlinal hinge of Villa Camilla and Castelvetro anticlines from Gasperi et al. (1999). Data source is a RER 10-m Elevation Dataset.

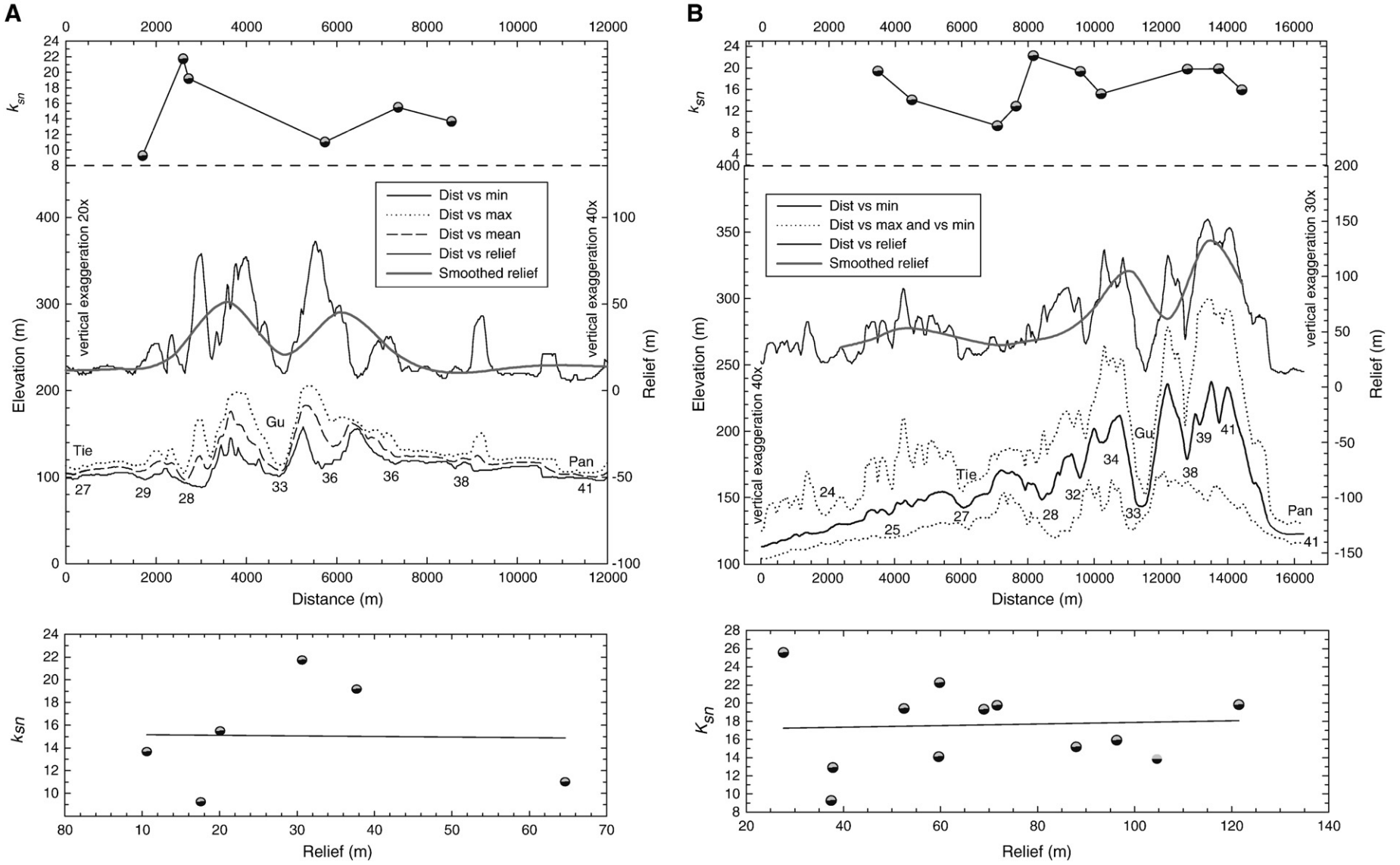

Fig. 7. Swath and relief profiles of topography related to k_{sn} trend along the anticlinal hinges of Castelvetro (A) and Villa Camilla anticlines (B). On top is plotted the trend of the maximum k_{sn} values calculated in the channel reaches crossing the anticline; in the centre, swath and relief profiles are plotted, with slowly different vertical scale: relief is plotted also as a smoothed profile obtained forcing for number and position of the streams that generate k_{sn} values; the plot at the bottom represents, at scale of a single structure, the relationship between maximum k_{sn} values and their relative relief. Data source is a RER 10-m Elevation Dataset. Numbers correspond to stream numeration in k_{sn} analysis shown in Figs. 10 and 12. Location and extension of the topography boxes are shown in Fig. 2. Guerro River (Gu), Tiepido River (Tie), Panaro River (Pa).

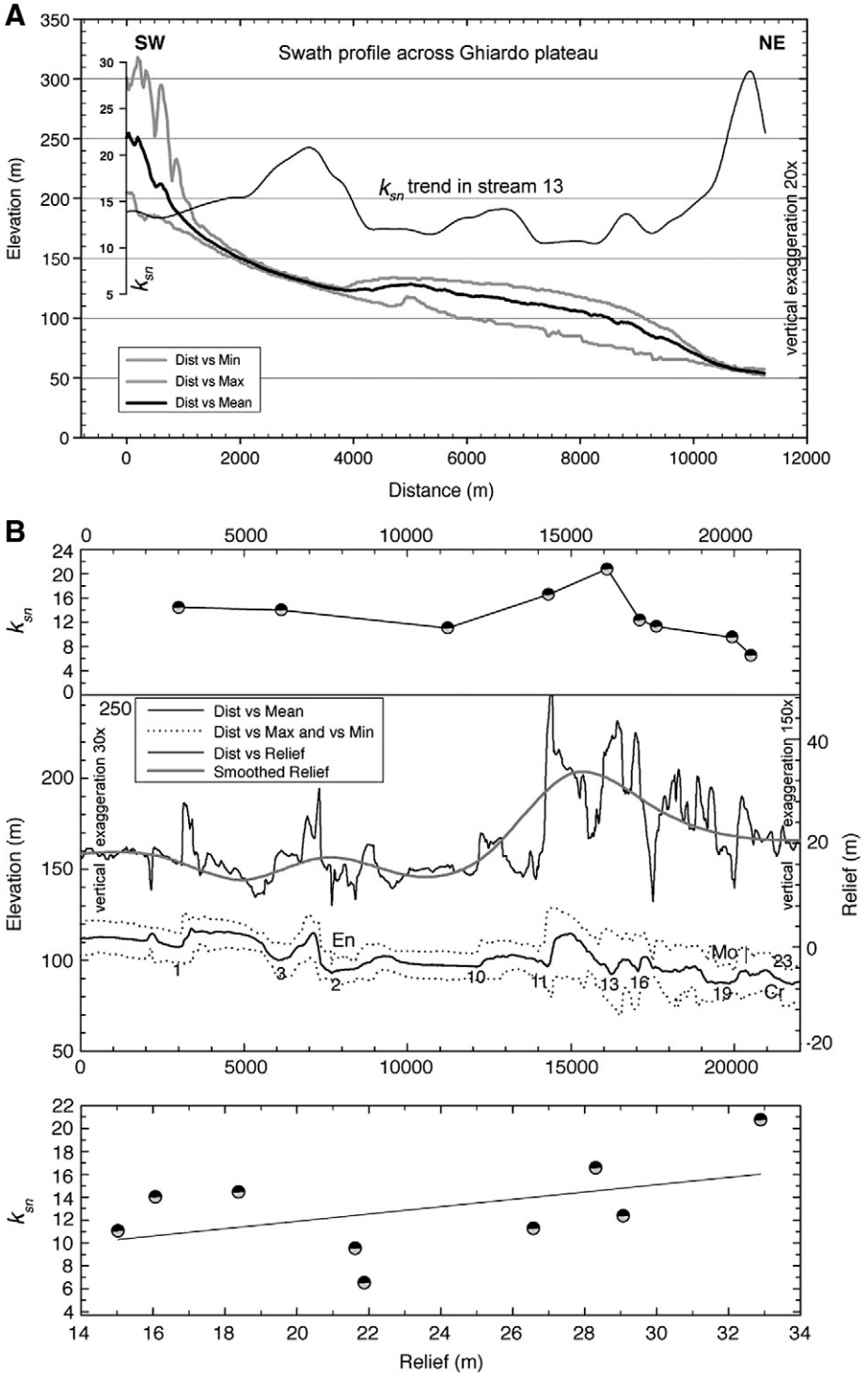

Fig. 8. A: Swath topographic profile perpendicular to anticlinal hinge of Ghiardo anticline. The location and extension (1 km wide) of the area of this swath profile is dashed in Fig. 3. Note in correspondence of the fold frontal limb, a zone of increasing in k_{sn} (see Fig. 10). B: Swath and relief profiles of topography related to k_{sn} trend along the anticlinal hinge of the Ghiardo anticline; on top is plotted the trend of the maximum k_{sn} values calculated in the channel reaches crossing the anticline; in the center, swath and relief profiles are plotted, with a great difference in vertical scale exaggeration: relief is plotted also as a smoothed profile obtained forcing for number and position of the streams that generate k_{sn} values; the plot at the bottom represents, at scale of a single structure, the relationship between maximum k_{sn} values and their relative relief. Data source is a RER 10-m Elevation Dataset. Numbers correspond to stream numeration in k_{sn} analysis shown in Figs. 10 and 12. Location and extension (2 km wide) of the swath are shown as a blue dashed box in Fig. 3. Enza River (En), Moddolena Creek (Mo), Crostolo Creek (Cr).

Rates of rock uplift are reconstructed from the deformation of stratigraphic and geomorphic markers of known age with respect to the local and regional elevation of those markers. The sedimentology of the Sabbie Gialle and lower AEI units allows us to assume original horizontality and an elevation at sea level at the time of deposition. The greater thickness of the AEI sediments infilling structural synclines with respect to those covering anticlinal hinges is due to local syndepositional subsidence and uplift, respectively. The fact

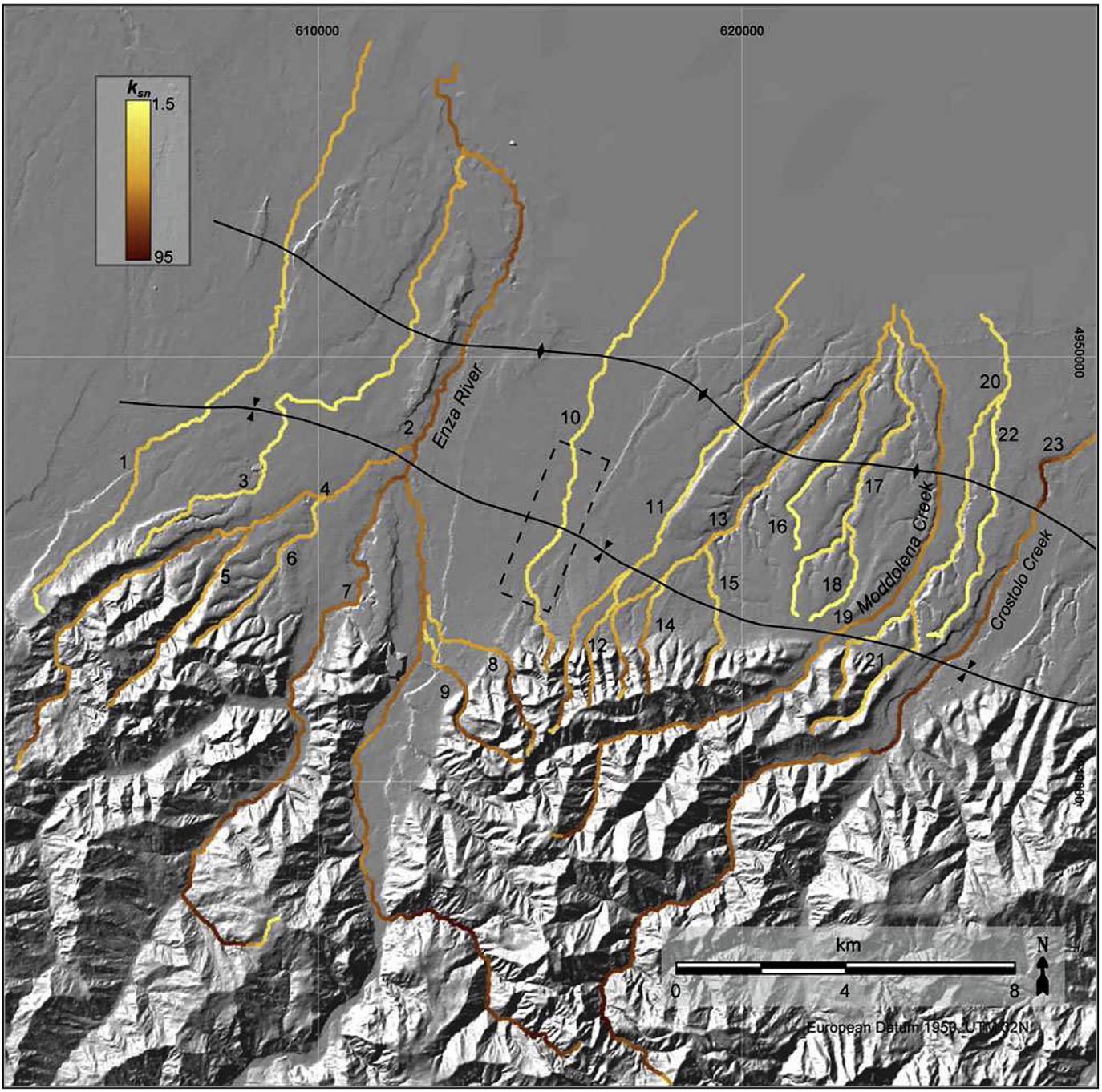

Fig. 9. Map of k_{sn} index color-coded to magnitude in hill-shaded topography of the Ghiardo plateau. Yellow–orange to dark red color scales from lowest to highest k_{sn} value. Dashed box shows an example of stream reaches about 3–4 km long straddling the fold axes and examined in Tables 2 and 3.

that AEI unit displays this growth strata constrain a minimum age for the activity of fold growth.

3.2. Swath profile

Swath-averaged topographic profiles provide a useful way to characterize the topography of orogenic belts where along-strike variations are small (Isacks, 1992). The difference between the maximum and minimum envelopes represents a measure of the local relief at length scales of the order of the swath width (Masek et al., 1994). In this technique a topographic profile is taken perpendicular to the strike, and all elevations within a specified swath width are projected into the plane of the section. Curves may then be constructed outlining the maximum, minimum, and the average elevations within the swath. Our analysis follows the general protocols outlined in Molin et al. (2004). Swath topographic profiles centered on and paralleling an anticlinal hinge of a structure represent a means of assessing along-strike variations in elevation that may reflect underlying fold growth. For the same reason, extended swath topographic profiles oriented perpendicularly to a fold axis are constructed to reflect underlying fold growth perpendicular to strike direction. We use an ArcInfo script (M. Oskin, affiliation personal

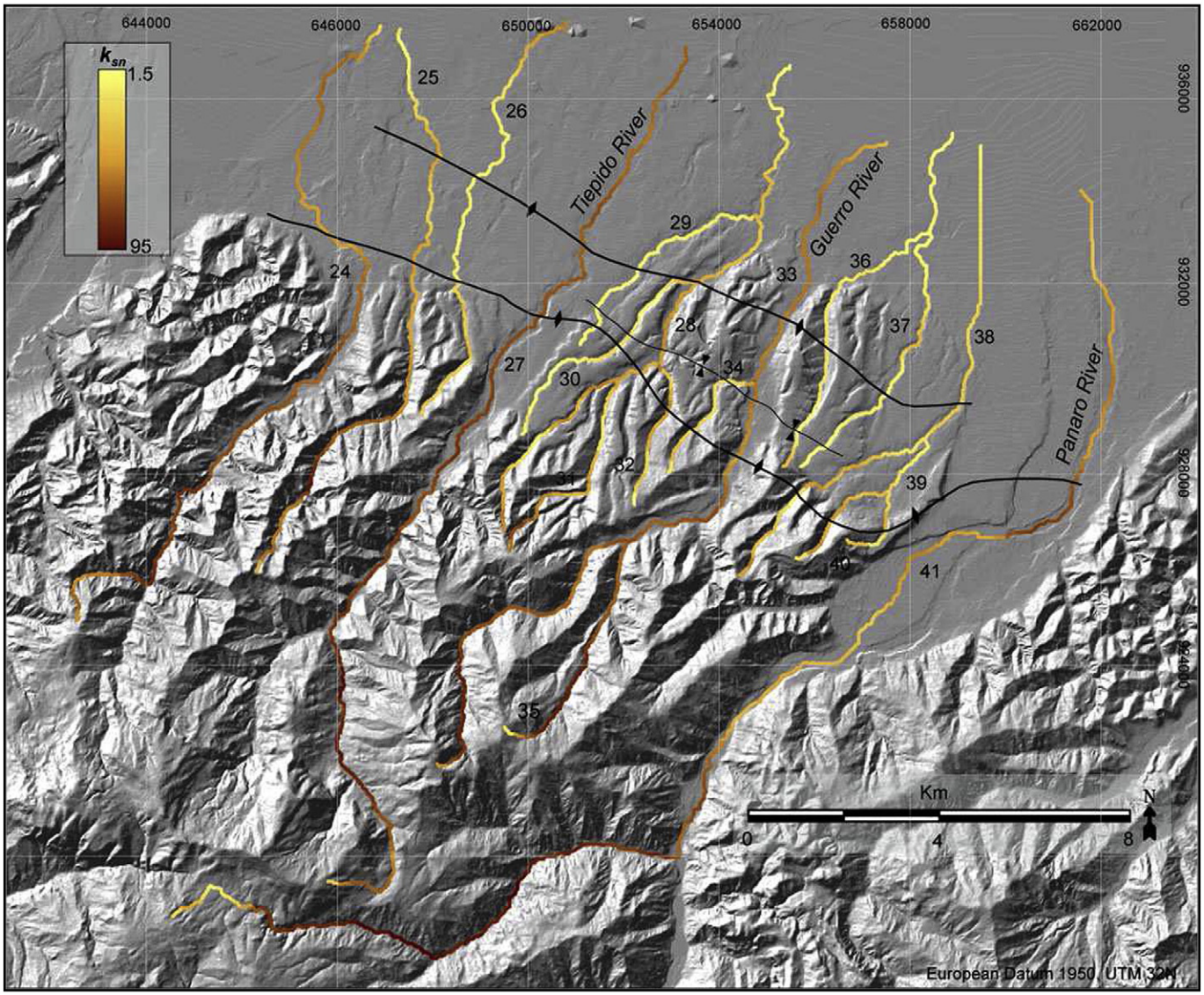

Fig. 10. Layout of color-coded stream segments based on their normalized steepness indices in Castelvetro–Vignola foothills. Yellow–orange to dark red color scales from lowest to highest k_{sn} value.

communication, 2007) that extracts topography data from the 10-m resolution DEM along a defined number of parallel profile lines, variable from 1 to 5 km in width and spaced 20 m apart orthogonally to the folds. Our swath profiles show minimum, maximum, and average elevations, relief, and smooth relief. We use a lowess filter on the relief to produce a smooth relief profile that captures the general trends. We fix the number of output points in the filter to the number of streams with calculated steepness values (see below) so that we can directly compare relief to steepness.

3.3. k_{sn} steepness index

Many studies (Hack, 1957, Flint, 1974; Snyder et al., 2000; Kirby and Whipple, 2001) have empirically observed in diverse geologic settings that the channel slope along a river tends to decrease inversely with the increase of the drainage area, defined by a power law in the form:

$$S = k_S A^{-\theta} \tag{1}$$

where S is the local channel gradient (m/m); A is the upstream drainage area (m^2) and considered a good proxy for discharge; k_s and θ are, respectively, steepness and concavity, the slope and y-intercept of a log–log plot of S and A.

Rock uplift (Snyder et al., 2000; Kirby and Whipple, 2001), climate (Roe et al., 2002; Zaprowski et al., 2001), and bedrock (Duvall et al., 2004; Spagnolo and Pazzaglia, 2005) are known to impact profile concavity and steepness. These effects can be modeled when the bedrock channel erosional process is assumed to be detachment-limited and proportional to stream power,

$$E = KA^m S^n \tag{2}$$

where E is the rate of bedrock erosion, K is a proportionality constant that accounts for substrate resistance, A is basin area upstream of a given reach, S is channel reach slope, and m and n are scaling factors related to basin hydrology and base level of erosion respectively. Eq. (2) stems from the fundamental assumption that bedrock channel erosion scales with shear stress on the bed, shear stress can be expressed as the reach-scale product of flow depth and channel

Table 1
Topographic characteristics of channel profiles in the studied areas.[a]

Stream	Easting_headwater[b]	Northing_headwater[b]	Easting_mouth[b]	Northing_mouth[b]	Max_area (m^2)	Min_area (m^2)	Max_k_{sn}[c]	Min_k_{sn}[c]	Length (km)	Name
Ghiardo k_{sn} analysis										
1	603341.4	4944206.5	611001.4	4956786.5	1.55E+07	2.60E+04	14.9	6.6	17.78	
2[d]	616031.4	4933686.5	612811.4	4956206.5	1.98E+08	3.91E+04	70.6	17.7	32.80	Enza River
3	605821.4	4945546.5	613401.4	4954726.5	2.03E+07	2.16E+04	17.7	5.2	16.74	Rio Zola
4	602951.4	4940506.5	612171.4	4947896.5	2.53E+07	4.17E+04	37.2	11.2	15.39	Masdone Creek
5	605171.4	4941956.5	608281.4	4945786.5	3.94E+06	2.46E+04	25.9	12.2	5.97	Madolo Creek
6	607181.4	4943376.5	609961.4	4946576.5	5.54E+06	6.19E+04	18.1	9.5	5.48	Rio Lama
7	608841.4	4936706.5	611971.4	4947176.5	6.44E+07	4.48E+04	20.9	9.4	17.84	Termina Creek
8	614591.4	4940476.5	612511.4	4943556.5	2.58E+06	4.03E+04	34.3	8.7	5.23	
9	615021.4	4940856.5	612581.4	4944376.5	3.80E+06	5.19E+04	37.6	9.7	5.86	
10	615351.4	4942836.5	618921.4	4953446.5	1.15E+07	2.52E+04	21.6	6.3	13.77	Rio Montebellone
11	615621.4	4941306.5	621451.4	4951946.5	1.23E+07	1.04E+04	33.2	7.4	14.78	Rio della Moia
12	616411.4	4942006.5	617311.4	4944916.5	1.21E+06	3.50E+04	22.6	9.1	3.78	Rio Monticelli
13	617201.4	4942176.5	623591.4	4950976.5	3.38E+07	2.89E+04	28.7	10.4	13.78	Rio Quaresimo
14	617801.4	4942346.5	618151.4	4944666.5	1.07E+06	9.62E+04	34.9	8.3	16.52	
15	619101.4	4942516.5	619201.4	4945386.5	5.55E+06	3.04E+04	22.4	9.5	3.92	
16	621251.4	4945486.5	623031.4	4949586.5	3.21E+06	1.16E+04	15.5	1.9	5.97	Rio Caviolo
17	621301.4	4943936.5	623531.4	4950676.5	8.38E+06	1.40E+04	13.0	2.0	9.65	Rio Moreno
18	621591.4	4943806.5	622561.4	4945976.5	1.72E+06	2.83E+04	9.5	1.9	3.43	
19[d]	615741.4	4938716.5	623871.4	4950896.5	2.71E+07	2.65E+04	43.1	11.9	20.53	Moddolena Creek
20	622291.4	4942156.5	625801.4	4950866.5	1.29E+07	3.85E+04	19.0	5.9	12.26	
21	621701.4	4941366.5	624041.4	4944076.5	2.22E+06	4.11E+04	17.0	9.1	4.81	
22	624571.4	4943486.5	626061.4	4948926.5	2.94E+06	2.19E+04	9.7	3.3	7.21	
23[d]	618131.4	4933076.5	628261.4	4948076.5	8.42E+07	1.03E+04	68.8	16.3	25.70	Crostolo Creek
Castelvetro–Vignola k_{sn} analysis										
24	640576.1	4925148.0	646786.1	4937228.0	5.76E+07	4.85E+04	50.8	12.7	19.54	Fossa Creek
25	644386.1	4926178.0	647276.1	4937168.0	1.34E+07	4.06E+04	65.1	7.2	14.47	Grizzaga Creek
26	647816.1	4929448.0	650696.1	4937348.0	9.66E+06	5.07E+04	21.7	8.5	10.76	
27[d]	646006.1	4919438.0	653336.1	4936718.0	5.09E+07	2.63E+04	80.1	13.3	24.30	Tiepido River
28	649636.1	4926628.0	655326.1	4936428.0	2.57E+07	4.06E+04	37.5	7.6	15.02	Nizzola Creek
29	651686.1	4931818.0	654706.1	4933388.0	3.63E+06	2.27E+04	14.9	6.3	5.42	
30	649946.1	4929038.0	653466.1	4932068.0	2.14E+06	1.56E+04	21.1	5.5	5.62	
31	650086.1	4928618.0	651666.1	4929928.0	3.24E+06	2.69E+04	23.2	9.9	4.47	
32	652246.1	4927598.0	652816.1	4930198.0	2.04E+06	2.83E+04	22.8	12.0	3.13	
33[d]	648276.1	4921918.0	657326.1	4934898.0	3.44E+07	4.57E+04	61.6	14.8	20.53	Guerro Creek
34	653006.1	4928258.0	654716.1	4929928.0	2.14E+06	1.20E+04	33.1	11.1	3.05	
35	649666.1	4922568.0	652056.1	4926558.0	7.78E+06	2.25E+04	60.7	20.7	5.58	
36	654586.1	4926028.0	659486.1	4934638.0	9.20E+06	3.49E+04	21.5	8.3	12.28	Rio Schiaviroli
37	655476.1	4928338.0	658786.1	4934938.0	1.18E+07	4.02E+04	13.4	7.3	9.27	
38	655876.1	4928318.0	658426.1	4933088.0	4.43E+06	4.46E+04	15.5	6.4	6.77	Rio Pissarotta
39	655806.1	4926338.0	658376.1	4928588.0	3.10E+06	4.37E+04	19.8	9.0	4.18	
40	656876.1	4926538.0	657546.1	4927638.0	7.01E+05	3.74E+04	15.9	10.4	1.75	
41[d]	642726.1	4918908.0	661736.1	4933768.0	1.03E+08	2.81E+04	93.6	9.9	34.54	Panaro River

[a] Read 1.6E + 07 as 1.6×10^7.
[b] Spatial reference of data Projection: European Datum 1950 Transverse Mercator, fuse 32N.
[c] Calculated with $\theta_{ref} = 0.45$.
[d] Main local rivers and creeks.

gradient, that discharge grows linearly with basin area, and that channel width increases downstream as the square root of the discharge (e.g. Snyder et al, 2000).

The steady-state profile requires that vertical river incision (E) be perfectly balanced by rock uplift (base level fall, U) such that the elevation of the channel is steady ($dz/dt = 0$),

$$dz/dt = U - E = 0 \quad (3)$$

Substituting Eqs. (2) into (3) and solving for S yields

$$S = (U/K)^{(1/n)} A^{(-m/n)} \quad (4)$$

where

$$k_S = (U/K)^{(1/n)}. \quad (5)$$

Eqs. (1) and (4) have the form of a straight line when plotted on logarithmic axes. Tectonics, expressed as the rate of rock uplift (U), is reflected in the profile steepness (k_s), and basin hydrology is primarily reflected as the profile concavity ($-m/n = \theta$).

Covariance between profile steepness and rock uplift is true only if (i) the river profile is in steady state with respect to current climatic and uplift conditions; and (ii) both uplift rate (U) and coefficient of erosion (K) are uniform through the channel reach (Whipple and Tucker, 1999; Kirby and Whipple, 2001; Sklar and Dietrich, 2001, 2004; Finnegan et al., 2005). Where these conditions are met, the parameters $(U/K)^{1/n}$ and m/n can be estimated directly through regressions of channel gradient and drainage area data (Snyder et al., 2000).

Deviations from the idealized steady-state profile are generally taken to be transient adjustments to a tectonic or environmental change and are expressed in quantifiable changes in concavity and steepness.

All topographic data (profiles, stream network and indexes) are extracted from the Regione Emilia–Romagna (RER) 10 m digital elevation model (DEM). The method of data extraction we apply comes directly from the "New Tools for Quantitative Geomorphology: Extraction and Interpretation of Stream Profiles from Digital Topographic Data" (Whipple et al., 2007). Those tools provide for a dual,

interfaced, and user-interactive ArcGIS-Matlab environment. We model channel profile steepness for the drainage network, small channels and rivers, crossing the described tectonic structures in the Ghiardo plateau and at the Castelvetro–Vignola foothills (Figs. 2 and 3). Streams 23 and 18 have been analyzed in the Ghiardo plateau and at Castelvetro–Vignola, respectively.

Following sensitivity analyses (Spagnolo and Pazzaglia, 2005), we use a moving average window of 0.25 km in length that allows us to smooth raw elevation data prior to calculating channel slopes over a specified vertical interval. Regressing the slope versus area plot over a user-specified moving window of 0.25 km (Auto k_sn window in the tool), the normalized channel steepness indices k_{sn} (y-intercept of the regression fit), varying along channel segments (Fig. 5), were extracted. Normalized steepness indexes (k_{sn}) have been calculated for a reference channel concavity (θ_{ref}) required for inter-channel interpretation and comparison. We choose a value for θ_{ref} of 0.45, equal to the mean of observed concavity values in channel segments in this study area and is in agreement with what it was used in previous studies (e.g., Snyder et al., 2003; Duvall et al., 2004; Wobus et al., 2006). In principle, however, relative differences in k_{sn} do not depend on the choice of θ_{ref} (Wobus et al., 2006). Our analysis and previous studies (Harkins et al., 2007) show that modeled k_{sn} values can change abruptly for adjacent channel reaches. In an effort to reveal the general trends in k_{sn} values, we adopt a smoothing protocol that, averaging through a 5-k_{sn}-value moving window (1.25 km long), localizes the maximum and minimum k_{sn} value in the meanly highest and lowest 5-k_{sn}-value-long reach of the stream, respectively.

We plot the data in mapview with color-coded stream segments based on their normalized k_{sn} that allows us to look at patterns of steepness indices within catchments and to identify transients related to continued growth of the structures. The k_{sn} coded map are colored following a geometrical statistical distribution of the values such that chromatic gradation intervals are scaled to be able to better visualize changes in k_{sn} across the critical areas. The smoothed maximum and minimum k_{sn} values are plotted in each stream as black stars and white dots.

4. Results

4.1. Tectonic setting

The geologic section AA′ crosses folded Middle Pleistocene growth strata (AEI, Qt1, and Qt2 in Picotti and Pazzaglia, 2008, and Wegmann and Pazzaglia, 2009) of the Ghiardo plateau from SW to NE (Figs. 3 and 4). The strata tilt to the SW at the mountain front and to

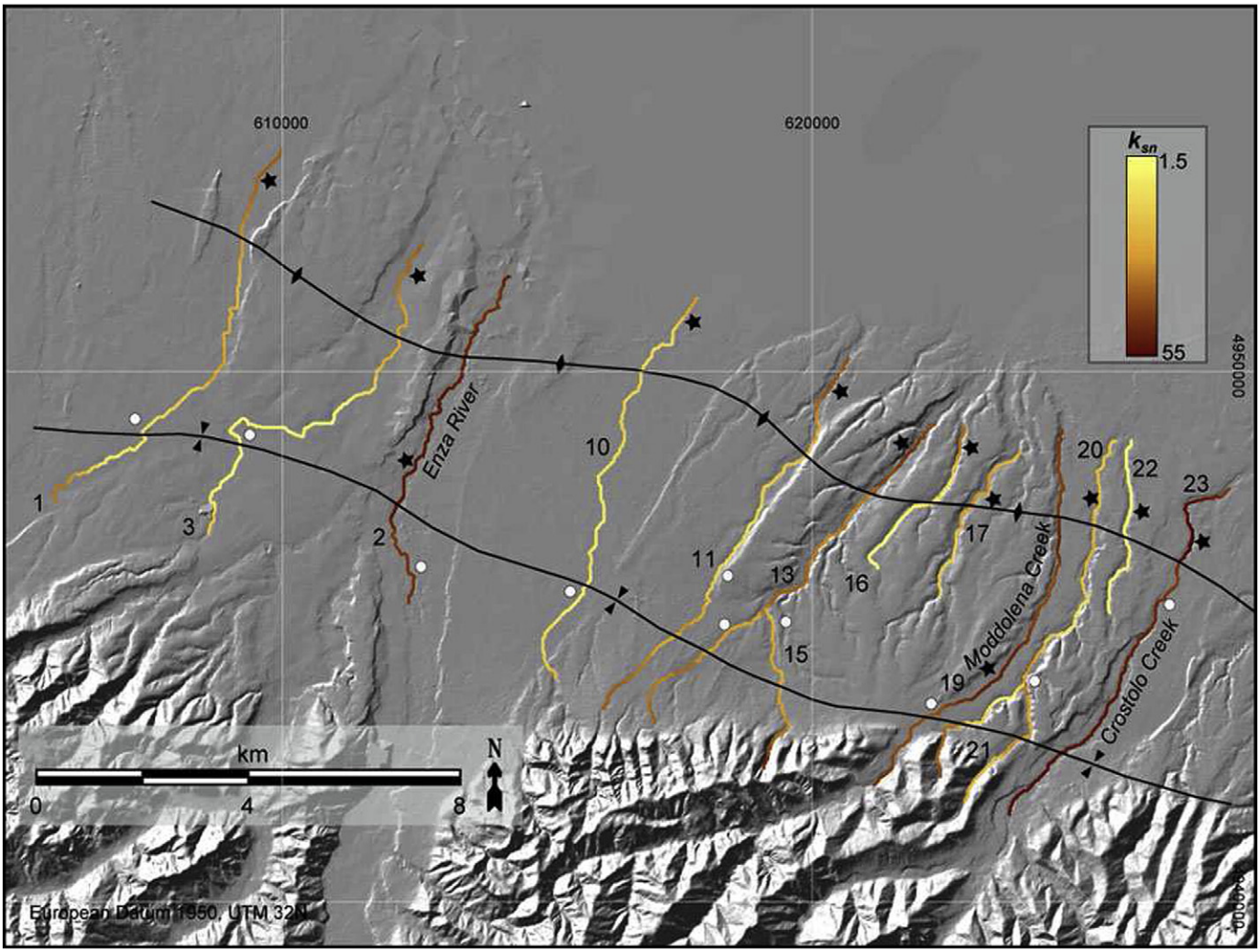

Fig. 11. Selected channel reaches crossing the active structures in the Ghiardo plateau: yellow–orange to dark red color-coded to magnitude spectrum have been here regularly graduated from k_{sn} 1.5 to 55. Black stars mark maximum values of k_{sn} smoothed for a 5-k_{sn}-value moving window, while white dots mark minimum values of k_{sn} smoothed for a 5-k_{sn}-value moving window. Drainage areas of the examined stream reaches straddling the fold axes do not exceed 170 km^2.

the NE on top of the Ghiardo anticline, where they onlap the underlain folded Sabbie Gialle. A measured section in the Enza River at San Polo d'Enza, subsurface seismic reflection data (Ponza, 2010, PhD dissertation) and the SP3 borehole stratigraphy published by Carnicelli et al. (2003) have been integrated to locally calibrate the thickness of the Quaternary deposits. The difference in stratigraphic thickness of the AEI gives an uplift rate for the Ghiardo anticline of ~0.28 mm/year. The current elevation of the Ghiardo plateau surface (110 m asl), assuming no erosion, indicates a long-term uplift rate of the anticline of ~0.18 mm/year since the close of AEI deposition. Similarly, the Castelvetro and Villa Camilla anticlines have uplift rates ranging from 0.29 ± 0.05 averaged in the last 230 ka and 0.1–0.2 mm/year in since the Middle Pleistocene, respectively (Ponza, 2010, PhD dissertation).

4.2. Swath profiles

We compare swath profiles oriented orthogonal to the anticline hinge of the Castelvetro, Villa Camilla, and Ghiardo anticlines (see Figs. 6 and 8A) to those erected parallel to their anticlinal hinges (Figs. 7A, B, and 8B). In the Castelvetro area, the mean and the maximum topography of the fold-orthogonal swaths (Fig. 6) describe two folds that rise abruptly in elevation toward the SW. In contrast, the minimum topography (the stream valleys actually) is graded to a common elevation. The minimum, mean, and maximum topography profiles of the fold-axis parallel line (Fig. 7A) show a general NW–SE uniform growth culminating at the intersection of the Guerro River valley, except for a small spike (km 9.1) that increases in elevation ~2 km east of the Panaro valley (Fig. 2). These profiles clearly show that the valley bottom of the major transverse rivers (the numbers in the figure correlate with the stream numeration in Figs. 10 and 12), dissecting the topography, are not at the same elevation, with the valley of the Guerro which stands the highest.

The Castelvetro anticline has its greatest relief of ~50 m in the structural core, with both elevation and relief decreasing along strike to the fold tips (Fig. 7A). In contrast, relief in the more hinterland Villa Camilla anticline is greatest in the eastern part of the structure at about 100 m, declining unsteadily to the west to less than 50 m (Fig. 7B).

The NE–SW oriented swath profile across the Ghiardo plateau (see Fig. 8A) parallels and includes the geologic section of Fig. 4 (see location and relative kilometric profile in Fig. 3). Starting from the high topography of the SW, the minimum mean and maximum profiles abruptly decrease in elevation describing a clear synclinal shape NE into the Po plain, whereas the mean and maximum topography growth in the well known Ghiardo antiform, the minimum topography (corresponding to the valley bottom of stream 13) lies several meters beneath the maximum and mean values. The along-strike swath (see Fig. 8B) shows a decrease in mean elevation, but increase in relief in the eastern half of the anticline. Relief grows abruptly 10 to 20 m approximately at the midpoint of the anticlinal trace.

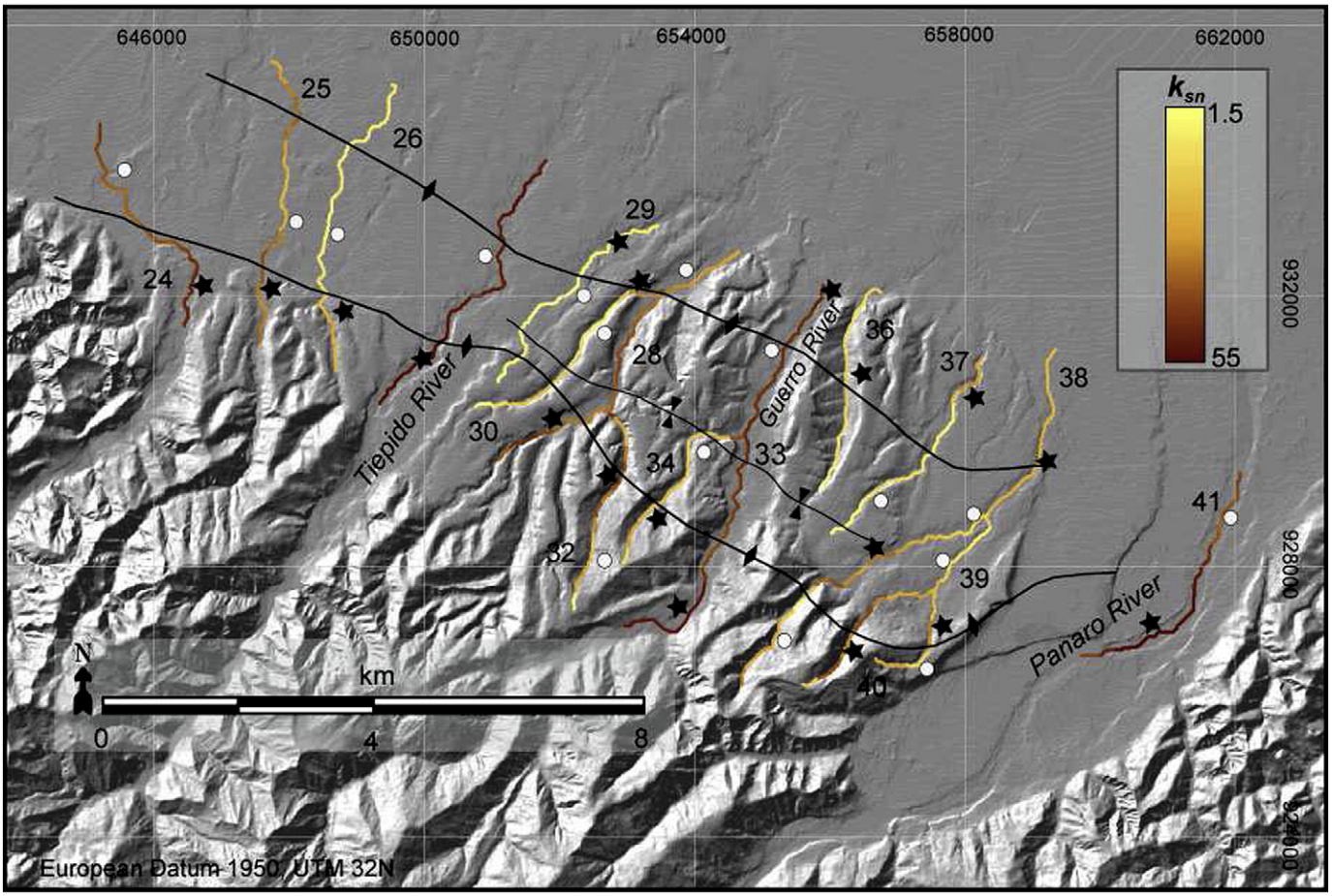

Fig. 12. Selected channel reaches crossing the active structures in the Castelvetro–Vignola foothills: yellow–orange to dark red color-coded to magnitude spectrum is here regularly graduated from k_{sn} 1.5 to 55. Black stars mark maximum values of k_{sn} smoothed for a 5-k_{sn}-value moving window, while white dots mark minimum values of k_{sn} smoothed for a 5-k_{sn}-value moving window. Drainage areas of the examined stream reaches straddling the fold axes do not exceed 170 km^2.

Table 2
Variations of k_{sn} along selected channel reaches, crossing the active tectonic structures on the Ghiardo plateau.

Stream	Easting[a]	Northing[a]	Min_area[b]	Max_area[b]	k_{sn}[c]	Easting[a]	Northing[a]	Min_area[b]	Max_area[b,c]	k_{sn}[c]
1	606071.4	948056.5	3.2E+06	3.3E+06	9.95	609031.4	951046.5	9.7E+06	9.7E+06	9.81
1	606301.4	948096.5	3.3E+06	3.3E+06	8.23	609061.4	951196.5	9.7E+06	9.8E+06	9.54
1	606511.4	948216.5	3.3E+06	3.3E+06	6.95	609161.4	951356.5	9.8E+06	9.9E+06	9.30
1	606671.4	948346.5	3.3E+06	3.4E+06	6.69	609151.4	951596.5	9.9E+06	1.2E+07	9.45
1	606901.4	948406.5	3.4E+06	3.5E+06	6.87	609201.4	951826.5	1.2E+07	1.2E+07	9.84
1	607091.4	948536.5	3.5E+06	3.9E+06	7.08	609201.4	952076.5	1.2E+07	1.3E+07	10.36
1	607291.4	948606.5	3.9E+06	3.9E+06	7.18	609241.4	952306.5	1.3E+07	1.4E+07	10.86
	Syncline				►◄	Anticline				◄►
1	607381.4	948786.5	3.9E+06	4.2E+06	7.38	609241.4	952546.5	1.4E+07	1.4E+07	11.27
1	607451.4	948966.5	4.2E+06	4.3E+06	7.68	609251.4	952786.5	1.4E+07	1.4E+07	11.81
1	607641.4	949136.5	4.3E+06	4.3E+06	7.97	609331.4	952996.5	1.4E+07	1.4E+07	12.25
1	607841.4	949246.5	4.3E+06	4.4E+06	8.26	609391.4	953216.5	1.4E+07	1.4E+07	12.89
1	608031.4	949396.5	4.4E+06	4.4E+06	8.57	609511.4	953416.5	1.4E+07	1.4E+07	13.41
1	608211.4	949576.5	4.4E+06	4.5E+06	8.70	609531.4	953666.5	1.4E+07	1.4E+07	13.97
1	608411.4	949686.5	4.5E+06	4.5E+06	9.24	609701.4	953836.5	1.4E+07	1.4E+07	14.46
2	612381.4	945626.5	6.7E+07	6.7E+07	21.18	612771.4	948826.5	1.6E+08	1.6E+08	29.03
2	612451.4	945846.5	6.7E+07	6.8E+07	21.01	612811.4	949046.5	1.6E+08	1.6E+08	28.83
2	612471.4	946086.5	6.8E+07	6.8E+07	20.88	612891.4	949196.5	1.6E+08	1.6E+08	28.60
2	612371.4	946236.5	6.8E+07	6.8E+07	20.78	612941.4	949356.5	1.6E+08	1.6E+08	28.22
2	612361.4	946476.5	6.8E+07	6.9E+07	20.66	613041.4	949566.5	1.6E+08	1.6E+08	27.57
2	612211.4	946606.5	6.9E+07	6.9E+07	20.42	613211.4	949706.5	1.6E+08	1.6E+08	26.57
2	612141.4	946826.5	6.9E+07	6.9E+07	20.53	613351.4	949876.5	1.6E+08	1.6E+08	25.27
2	612111.4	947026.5	6.9E+07	1.3E+08	24.01	613411.4	950106.5	1.6E+08	1.6E+08	24.10
	Syncline				►◄	Anticline				◄►
2	612041.4	947236.5	1.3E+08	1.3E+08	27.39	613461.4	950316.5	1.6E+08	1.7E+08	23.44
2	612141.4	947456.5	1.3E+08	1.3E+08	27.51	613531.4	950526.5	1.7E+08	1.7E+08	22.77
2	612281.4	947636.5	1.3E+08	1.3E+08	28.55	613641.4	950726.5	1.7E+08	1.7E+08	22.02
2	612301.4	947876.5	1.3E+08	1.6E+08	29.83	613701.4	950916.5	1.7E+08	1.7E+08	21.50
2	612381.4	948076.5	1.6E+08	1.6E+08	29.95	613831.4	951096.5	1.7E+08	1.7E+08	21.26
2	612511.4	948246.5	1.6E+08	1.6E+08	29.79	614041.4	951196.5	1.7E+08	1.7E+08	21.11
2	612651.4	948396.5	1.6E+08	1.6E+08	29.50	614111.4	951396.5	1.7E+08	1.7E+08	21.78
3	608681.4	947176.5	1.8E+06	1.8E+06	8.08	611281.4	949476.5	7.9E+06	8.6E+06	6.93
3	608731.4	947396.5	1.8E+06	2.3E+06	7.07	611491.4	949576.5	8.6E+06	1.0E+07	7.67
3	608641.4	947576.5	2.3E+06	2.4E+06	6.48	611711.4	949676.5	1.0E+07	1.0E+07	8.63
3	608741.4	947776.5	2.4E+06	2.4E+06	5.98	611761.4	949896.5	1.0E+07	1.1E+07	9.61
3	608881.4	947936.5	2.4E+06	2.6E+06	5.69	611871.4	950096.5	1.1E+07	1.1E+07	10.11
3	609061.4	948096.5	2.6E+06	3.4E+06	5.48	612001.4	950256.5	1.1E+07	1.2E+07	10.20
3	609141.4	948316.5	3.4E+06	3.6E+06	5.22	612161.4	950426.5	1.2E+07	1.2E+07	10.25
3	609211.4	948516.5	3.6E+06	4.5E+06	5.34	Anticline				◄►
	Syncline				►◄	612201.4	950656.5	1.2E+07	1.2E+07	10.29
3	609181.4	948756.5	4.5E+06	4.6E+06	5.81	612251.4	950856.5	1.2E+07	1.3E+07	10.31
3	609001.4	948886.5	4.6E+06	6.0E+06	6.12	612341.4	951036.5	1.3E+07	1.3E+07	10.33
3	609181.4	949066.5	6.0E+06	6.0E+06	6.04	612261.4	951256.5	1.3E+07	1.3E+07	11.16
3	609341.4	949036.5	6.0E+06	6.2E+06	5.95	612171.4	951446.5	1.3E+07	1.6E+07	12.26
3	609551.4	948966.5	6.2E+06	6.2E+06	5.78	612221.4	951666.5	1.6E+07	1.7E+07	12.76
3	609801.4	948946.5	6.2E+06	6.2E+06	5.72	612331.4	951856.5	1.7E+07	1.7E+07	13.23
3	610041.4	948946.5	6.4E+06	6.8E+06	5.90	612391.4	952056.5	1.7E+07	1.7E+07	13.64
3	610241.4	948816.5	6.8E+06	7.7E+06	6.02	612521.4	952226.5	1.7E+07	1.7E+07	14.04
3	610401.4	948866.5	7.7E+06	7.7E+06	6.02					
3	610561.4	949006.5	7.7E+06	7.7E+06	5.73					
3	610811.4	949016.5	7.7E+06	7.9E+06	5.27					
10	615161.4	944206.5	1.3E+06	1.3E+06	9.55	616371.4	948496.5	5.9E+06	6.1E+06	7.90
10	615071.4	944386.5	1.3E+06	1.4E+06	8.73	616451.4	948716.5	6.1E+06	6.2E+06	8.03
10	614941.4	944576.5	1.4E+06	1.4E+06	7.91	616421.4	948946.5	6.2E+06	6.2E+06	8.14
10	614911.4	944816.5	1.4E+06	1.4E+06	7.74	616421.4	949166.5	6.2E+06	6.2E+06	8.26
10	614961.4	945036.5	1.5E+06	2.0E+06	7.82	616451.4	949406.5	6.2E+06	6.3E+06	8.31
10	615101.4	945226.5	2.0E+06	2.0E+06	7.12	616611.4	949596.5	6.4E+06	6.5E+06	8.16
10	615271.4	945406.5	2.0E+06	2.1E+06	6.54	616751.4	949756.5	6.5E+06	6.5E+06	7.98
10	615461.4	945566.5	2.1E+06	2.2E+06	6.29	Anticline				◄►
	Syncline				►◄	616781.4	949996.5	6.5E+06	6.5E+06	7.74
10	615621.4	945746.5	2.2E+06	2.9E+06	6.38	616891.4	950196.5	6.5E+06	6.6E+06	7.54
10	615701.4	945936.5	2.9E+06	2.9E+06	6.85	617001.4	950396.5	6.6E+06	6.9E+06	7.48
10	615821.4	946136.5	2.9E+06	4.4E+06	7.26	617181.4	950526.5	6.9E+06	7.5E+06	7.52
10	615821.4	946386.5	4.4E+06	4.4E+06	7.20	617361.4	950586.5	7.5E+06	7.5E+06	7.87
10	615801.4	946606.5	4.4E+06	5.2E+06	7.04	617401.4	950816.5	7.5E+06	8.9E+06	8.99
10	615911.4	946786.5	5.2E+06	5.3E+06	6.84	617561.4	951006.5	8.9E+06	9.0E+06	10.16
10	615931.4	947026.5	5.3E+06	5.4E+06	6.72	617691.4	951196.5	9.0E+06	9.2E+06	11.06
11	616441.4	944146.5	1.5E+06	1.6E+06	13.48	618951.4	947286.5	6.2E+06	6.3E+06	7.86
11	616621.4	944286.5	1.6E+06	1.6E+06	12.62	619051.4	947486.5	6.3E+06	6.5E+06	8.05
11	616801.4	944456.5	1.6E+06	1.7E+06	11.66	619061.4	947726.5	6.5E+06	6.6E+06	8.21
11	616951.4	944636.5	1.7E+06	1.7E+06	10.52	619201.4	947876.5	6.6E+06	6.6E+06	8.45
11	617111.4	944826.5	1.7E+06	1.7E+06	10.17	619381.4	948046.5	6.8E+06	6.9E+06	8.72
11	617311.4	944946.5	1.7E+06	3.0E+06	10.98	619511.4	948236.5	6.9E+06	7.0E+06	9.02
11	617511.4	945066.5	3.0E+06	3.0E+06	11.30	619721.4	948306.5	7.0E+06	7.2E+06	9.33
	Syncline				►◄	Anticline				◄►

Table 2 (*continued*)

Stream	Easting[a]	Northing[a]	Min_area[b]	Max_area[b]	k_{sn}[c]	Easting[a]	Northing[a]	Min_area[b]	Max_area[b,c]	k_{sn}[c]
11	617671.4	945236.5	3.0E+06	3.2E+06	10.74	619901.4	948446.5	7.2E+06	7.3E+06	9.56
11	617871.4	945356.5	3.2E+06	3.3E+06	10.07	620011.4	948646.5	7.3E+06	7.4E+06	9.72
11	617961.4	945556.5	3.3E+06	3.4E+06	9.31	620091.4	948856.5	7.4E+06	7.5E+06	10.11
11	618011.4	945736.5	3.4E+06	3.6E+06	8.49	620111.4	949066.5	7.5E+06	7.6E+06	11.37
11	618111.4	945936.5	3.7E+06	3.9E+06	8.10	620111.4	949286.5	7.6E+06	9.8E+06	13.51
11	618191.4	946156.5	3.9E+06	4.3E+06	7.81	620171.4	949486.5	9.8E+06	1.0E+07	15.66
11	618301.4	946356.5	4.3E+06	4.4E+06	7.59	620321.4	949676.5	1.0E+07	1.0E+07	16.57
11						620451.4	949866.5	1.0E+07	1.0E+07	16.17
13	617011.4	944016.5	1.2E+06	1.3E+06	11.70	620041.4	946526.5	1.4E+07	1.4E+07	11.69
13	617161.4	944186.5	1.3E+06	1.3E+06	11.88	620151.4	946716.5	1.4E+07	1.4E+07	11.42
13	617371.4	944286.5	1.3E+06	1.3E+06	13.32	620311.4	946896.5	1.4E+07	1.7E+07	11.76
13	617581.4	944376.5	1.3E+06	1.9E+06	13.34	620511.4	946986.5	1.7E+07	1.7E+07	11.99
13	617771.4	944516.5	1.9E+06	2.0E+06	11.47	620631.4	947166.5	1.7E+07	1.7E+07	11.98
13	617921.4	944656.5	2.0E+06	2.0E+06	10.43	620761.4	947366.5	1.7E+07	1.8E+07	12.01
13	618121.4	944766.5	2.0E+06	3.2E+06	10.63	620931.4	947526.5	1.8E+07	1.8E+07	12.15
	Syncline				►◄	Anticline				◄►
13	618271.4	944936.5	3.2E+06	3.2E+06	10.69	621071.4	947716.5	1.8E+07	1.8E+07	14.26
13	618431.4	945126.5	3.2E+06	3.3E+06	10.59	621241.4	947816.5	1.8E+07	1.9E+07	16.85
13	618641.4	945206.5	3.3E+06	3.7E+06	10.49	621421.4	947996.5	1.9E+07	1.9E+07	17.96
13	618851.4	945266.5	3.8E+06	3.8E+06	10.77	621591.4	948176.5	1.9E+07	1.9E+07	20.12
13	619011.4	945446.5	3.8E+06	9.5E+06	12.56	621731.4	948356.5	1.9E+07	1.9E+07	20.77
13	619191.4	945606.5	9.5E+06	9.5E+06	13.96	621901.4	948526.5	1.9E+07	1.9E+07	20.07
13	619311.4	945786.5	9.5E+06	1.1E+07	14.14	622021.4	948716.5	1.9E+07	1.9E+07	19.24
15	619101.4	942516.5	3.0E+04	1.8E+05	22.25	621081.4	946466.5	5.9E+05	6.8E+05	4.79
15	619171.4	942726.5	1.9E+05	2.8E+05	16.81	621211.4	946666.5	6.8E+05	7.7E+05	4.69
15	619211.4	942946.5	2.8E+05	3.5E+05	13.32	621371.4	946816.5	7.7E+05	1.1E+06	4.99
15	619351.4	943136.5	3.5E+05	4.4E+05	12.35	621531.4	947006.5	1.1E+06	1.2E+06	5.64
15	619531.4	943286.5	4.5E+05	7.0E+05	11.52	621651.4	947196.5	1.2E+06	1.4E+06	6.17
15	619481.4	943496.5	7.0E+05	7.5E+05	10.90	621831.4	947376.5	1.4E+06	1.4E+06	6.55
15	619431.4	943716.5	7.5E+05	1.4E+06	10.67	622041.4	947476.5	1.4E+06	1.5E+06	7.01
15	619391.4	943916.5	1.4E+06	1.4E+06	9.78	Anticline				◄►
	Syncline				►◄	622271.4	947526.5	1.9E+06	2.1E+06	7.48
15	619421.4	944156.5	1.4E+06	2.9E+06	9.83	622421.4	947676.5	2.1E+06	2.2E+06	7.45
15	619391.4	944346.5	2.9E+06	3.0E+06	10.30	622581.4	947866.5	2.2E+06	2.3E+06	7.60
15	619251.4	944506.5	3.0E+06	5.2E+06	10.45	622671.4	948076.5	2.3E+06	2.4E+06	9.17
15	619271.4	944716.5	5.2E+06	5.3E+06	10.32	622741.4	948296.5	2.4E+06	2.6E+06	11.39
15	619241.4	944936.5	5.3E+06	5.4E+06	9.91	622791.4	948526.5	2.6E+06	2.6E+06	12.16
15	619261.4	945166.5	5.4E+06	5.5E+06	9.52	622821.4	948766.5	2.7E+06	2.8E+06	12.38
15	619201.4	945386.5	5.5E+06	5.6E+06	9.83					
19	621161.4	942206.5	1.8E+07	1.8E+07	20.88	624451.4	945746.5	2.1E+07	2.1E+07	17.33
19	621331.4	942366.5	1.8E+07	1.8E+07	20.24	624521.4	945946.5	2.1E+07	2.1E+07	17.57
19	621511.4	942526.5	1.8E+07	1.8E+07	19.38	624581.4	946156.5	2.1E+07	2.1E+07	19.11
19	621521.4	942756.5	1.8E+07	1.9E+07	18.20	624681.4	946376.5	2.1E+07	2.2E+07	21.04
19	621681.4	942946.5	1.9E+07	1.9E+07	17.76	624631.4	946606.5	2.2E+07	2.2E+07	22.62
19	621851.4	943086.5	1.9E+07	1.9E+07	17.45	624671.4	946826.5	2.2E+07	2.3E+07	22.45
19	621911.4	943306.5	1.9E+07	1.9E+07	16.93	624671.4	947056.5	2.3E+07	2.3E+07	21.30
19	622101.4	943456.5	1.9E+07	1.9E+07	16.42	Anticline				◄►
	Syncline				►◄	624651.4	947306.5	2.3E+07	2.3E+07	20.05
19	622321.4	943536.5	1.9E+07	1.9E+07	16.95	624691.4	947536.5	2.3E+07	2.3E+07	19.05
19	622481.4	943656.5	1.9E+07	1.9E+07	19.00	624741.4	947766.5	2.3E+07	2.4E+07	18.59
19	622701.4	943736.5	1.9E+07	2.0E+07	21.57	624701.4	947976.5	2.4E+07	2.4E+07	18.84
19	622921.4	943806.5	2.0E+07	2.0E+07	23.36	624651.4	948196.5	2.4E+07	2.4E+07	19.31
19	623131.4	943916.5	2.0E+07	2.0E+07	23.99	624671.4	948436.5	2.4E+07	2.4E+07	19.87
19	623311.4	944066.5	2.0E+07	2.0E+07	24.22					
20	622291.4	942156.5	3.9E+04	1.8E+05	18.97	625171.4	945676.5	6.0E+06	6.3E+06	8.12
20	622431.4	942356.5	1.8E+05	2.8E+05	15.66	625141.4	945876.5	6.3E+06	6.4E+06	9.10
20	622401.4	942576.5	3.1E+05	4.4E+05	13.58	625101.4	946106.5	6.5E+06	6.6E+06	9.60
20	622391.4	942806.5	4.5E+05	5.4E+05	12.90	625161.4	946336.5	6.6E+06	6.7E+06	9.82
20	622471.4	943026.5	5.4E+05	5.9E+05	13.04	625251.4	946546.5	6.7E+06	6.8E+06	9.73
20	622501.4	943256.5	5.9E+05	8.4E+05	12.67	625301.4	946766.5	6.8E+06	6.9E+06	9.58
20	622691.4	943286.5	8.4E+05	9.8E+05	10.40	Anticline				◄►
	Siyncline				►◄	625321.4	947006.5	6.9E+06	7.1E+06	9.55
20	622891.4	943366.5	9.8E+05	1.3E+06	8.35	625331.4	947246.5	7.1E+06	7.2E+06	9.46
20	623121.4	943376.5	1.3E+06	1.5E+06	8.02	625411.4	947446.5	7.2E+06	7.3E+06	9.43
20	623271.4	943536.5	1.6E+06	1.7E+06	7.33	625441.4	947686.5	7.3E+06	7.6E+06	9.45
20	623411.4	943726.5	1.7E+06	1.7E+06	6.18	625411.4	947926.5	7.6E+06	7.7E+06	9.38
20	623621.4	943836.5	1.7E+06	2.0E+06	5.95	625391.4	948136.5	7.7E+06	7.8E+06	9.17
20	623831.4	943926.5	2.0E+06	2.0E+06	7.81	625511.4	948326.5	7.8E+06	7.9E+06	8.93
20	623991.4	944096.5	2.0E+06	4.4E+06	10.56	625631.4	948526.5	7.9E+06	8.0E+06	8.76
20	624041.4	944306.5	4.4E+06	4.9E+06	11.55					
23	623731.4	941626.5	6.9E+07	6.9E+07	37.91	626231.4	944986.5	7.6E+07	7.6E+07	22.16
23	623771.4	941856.5	7.0E+07	7.0E+07	37.95	626401.4	945166.5	7.6E+07	7.7E+07	22.17
23	623921.4	942036.5	7.0E+07	7.0E+07	37.57	626481.4	945386.5	7.7E+07	7.7E+07	21.93
23	624121.4	942166.5	7.0E+07	7.2E+07	36.42	626511.4	945626.5	7.7E+07	7.7E+07	21.17
23	624291.4	942336.5	7.2E+07	7.2E+07	34.98	626671.4	945776.5	7.7E+07	7.7E+07	19.93

(*continued on next page*)

Table 2 (*continued*)

Stream	Easting[a]	Northing[a]	Min_area[b]	Max_area[b]	k_{sn}[c]	Easting[a]	Northing[a]	Min_area[b]	Max_area[b,c]	k_{sn}[c]
23	624451.4	942506.5	7.2E+07	7.3E+07	33.46	626841.4	945946.5	7.7E+07	7.8E+07	18.49
23	624581.4	942696.5	7.3E+07	7.3E+07	31.00	626881.4	946156.5	7.8E+07	7.8E+07	20.85
	Syncline				►◄	Anticline				◄►
23	624761.4	942836.5	7.3E+07	7.4E+07	29.63	626921.4	946386.5	7.8E+07	7.8E+07	33.38
23	624951.4	942936.5	7.4E+07	7.4E+07	29.72	627051.4	946566.5	7.8E+07	8.1E+07	48.75
23	625141.4	943036.5	7.4E+07	7.4E+07	30.03	627161.4	946776.5	8.1E+07	8.1E+07	52.52
23	625281.4	943186.5	7.4E+07	7.5E+07	30.48	627181.4	947016.5	8.1E+07	8.2E+07	49.27
23	625431.4	943376.5	7.5E+07	7.5E+07	30.58	627091.4	947236.5	8.2E+07	8.2E+07	42.87
23	625551.4	943576.5	7.5E+07	7.5E+07	29.46	627061.4	947456.5	8.2E+07	8.2E+07	37.65
23	625651.4	943776.5	7.5E+07	7.5E+07	28.62	627251.4	947556.5	8.2E+07	8.2E+07	30.20
23						627481.4	947596.5	8.2E+07	8.3E+07	22.31
23						627701.4	947626.5	8.3E+07	8.4E+07	20.35

Stream	Easting[a]	Northing[a]	Max_area[b]	k_{sn}[c]	Stream	Easting[a]	Northing[a]	Max_area[b,c]	k_{sn}[c]
22	625621.4	945446.5	8.5E+05	6.63	17.0	622401.4	945786.5	1.6E+06	7.84
22	625601.4	945686.5	9.4E+05	5.29	17.0	622391.4	946016.5	3.4E+06	8.66
22	625611.4	945936.5	1.1E+06	5.56	17.0	622431.4	946226.5	3.5E+06	8.30
22	625721.4	946126.5	1.2E+06	5.95	17.0	622581.4	946416.5	4.1E+06	7.85
22	625881.4	946286.5	1.4E+06	6.38	17.0	622681.4	946596.5	4.2E+06	8.09
22	625961.4	946446.5	1.5E+06	6.53	17.0	622721.4	946836.5	4.3E+06	8.99
22	625981.4	946686.5	1.7E+06	6.39	17.0	622801.4	947046.5	4.4E+06	10.11
	Anticline			◄►	17.0	622821.4	947276.5	4.5E+06	10.90
22	625921.4	946906.5	1.8E+06	6.20		Anticline			◄►
22	625921.4	947136.5	2.0E+06	5.90	17.0	622981.4	947416.5	4.7E+06	11.29
22	626001.4	947346.5	2.0E+06	5.61	17.0	623101.4	947616.5	4.9E+06	10.89
22	626031.4	947576.5	2.1E+06	5.49	17.0	623271.4	947706.5	5.0E+06	10.63
22	626011.4	947816.5	2.2E+06	5.47	17.0	623351.4	947906.5	5.1E+06	10.45
22	625961.4	948036.5	2.3E+06	5.48	17.0	623421.4	948126.5	5.4E+06	9.92
22	625941.4	948256.5	2.3E+06	5.66	17.0	623601.4	948256.5	5.5E+06	9.62
					17.0	623811.4	5497400	5.5E+06	9.49

[a] Spatial reference of data Projection: European Datum 1950 Transverse Mercator, fuse 32N.
[b] Drainage area expressed in m^2. Read 3.2E+06 as 3.2×10^6.
[c] Calculated with $\theta_{ref}=0.45$.

4.3. Stream profile analysis: steepness indexes

The magnitudes of k_{sn} are plotted as color-coded maps in Figs. 9 and 10 (see Table 1 for all topographic characteristics of the streams). In both study areas, k_{sn} values tend to scale with the size of the channel. Large channels (such as the Enza, the Moddolena, the Crostolo, the Panaro, the Tiepido, and the Guerro) that have headwaters in the Emilia foothills, have higher overall k_{sn} values in comparison to smaller, commonly ephemeral streams that are sourced at the mountain front or in the Po plain.

For the smaller streams high k_{sn} values scale with the mapped locations of the anticlines; however, this general relationship does not exist for the larger drainages (Figs. 9 and 10). For example, in the Ghiardo plateau, the largest analyzed channel is a reach of the Enza River (stream 2 in Table 1) ~32 km long. It drains an area of ~200 km^2, with max k_{sn} value equal to 70.6 (highest registered steepness index in the area, see Fig. 9 and Table 1). The smallest stream is number 18, a tributary of stream 17, Rio Moreno (see Table 1), that develops ~3.43 km in length, with a drainage area of ~1.7 km^2 and with a max k_{sn} value of 9.5. Similarly, in the Castelvetro–Vignola area the largest analyzed channel is a reach of the Panaro River ~34 km long and with a maximum drainage area of ~103 km^2 and a maximum k_{sn} value of 93.6 (absolute maximum steepness index obtained by the stream analysis in this study). The smallest stream is number 40 (see Fig. 10 and Table 1), a tributary of the Rio Schiaviroli, ~1.7 km long, with a maximum drainage area of ~0.7 km^2 a maximum k_{sn} value of 15.9.

We focus on the subtle differences in k_{sn} in the region where the channels transverse to the structures. The corresponding reaches are about 3–4 km long, straddle the fold axes, and include 14 and 16 rivers across the Ghiardo and Castelvetro–Vignola structures, respectively, that have drainage areas in excess of 170 km^2 (Figs. 11 and 12; Tables 2 and 3). The general distribution of k_{sn} values is once again shown by a dark red–orange–yellow color ramp where darker red indicates steeper channels. For these channels, k_{sn} value ranges from 5 to 52 in the Ghiardo plateau and from 6.3 to 40 in Castelvetro–Vignola.

Black stars and white dots are plotted to show the maximum and minimum smoothed k_{sn} values respectively. In the Ghiardo plateau, most of the black stars fall on or a few hundreds of meters downstream of the mapped trace of the fold hinge, mostly in the fold frontal limb zone (see e.g., k_{sn} trend of stream 13 in Fig. 8A), while a large number of the white dots fall on or near the syncline axis. We note that a reach of the Crostolo Creek (stream 23) has k_{sn} values of 30–52, results that are anomalously high with respect to the regional values (see Table 2).

In the Castelvetro–Vignola foothills, the general location of the black stars lies mostly in the zone of highest topography, near or on the Villa Camilla fold axis, which stands in comparison to the Ghiardo plateau results. However, for five small streams, black stars fall on or near the Castelvetro fold hinge in the frontal limb area toward the Po plain. In contrast, the greater part of the white dots localize in the syncline zone, between the two anticlines, similar to their position in the Ghiardo area. Also similar to the Ghiardo area, stars and dots of the smaller streams with drainage area <20 km^2 fall closer to the axes of the structures then the larger streams such as the Panaro, the Guerro, and the Tiepido.

5. Discussion

The swath profiles (Figs. 6–8) and modeled long profile (k_{sn}, Figs. 7–12) data are consistent with the active tectonic forcing (Snyder et al., 2000; Kirby and Whipple, 2001) expected in a growing mountain front. Relief in the swath profiles is the result of fluvial dissection of uplifted topography and therefore stands as a general marker for rock uplift. In contrast channel k_{sn} values indicate where the channel long profile is steepest given a constant equilibrium concavity. Together, these data represent the integration of a geomorphic marker and morphometric approach in quantifying active tectonics. Below we explore the dependency between the development of relief and the k_{sn} values that

Table 3
Variations of k_{sn} along selected channel reaches crossing the active tectonic structures in the Castelvetro–Vignola foothills.

Stream	Easting[a]	Northing[a]	Min_area[b]	Max_area[b]	k_{sn}[c]
24	646456	931548	2.7E+07	2.7E+07	25.57
24	646496	931778	2.7E+07	2.7E+07	25.39
24	646496	931988	2.7E+07	2.7E+07	24.62
24	646556	932178	2.7E+07	2.7E+07	23.98
24	646646	932388	2.7E+07	2.7E+07	22.45
24	646536	932558	2.7E+07	2.7E+07	20.40
24	646406	932718	2.7E+07	2.8E+07	19.08
24	646196	932798	2.8E+07	2.8E+07	19.36
24	645986	932878	3.5E+07	3.5E+07	19.89
	Villa Camilla anticline				⟷
24	645806	933058	3.5E+07	3.5E+07	18.69
24	645636	933228	3.5E+07	3.6E+07	18.13
24	645606	933468	3.6E+07	3.6E+07	17.96
24	645466	933588	3.6E+07	3.6E+07	18.45
24	645266	933708	3.6E+07	3.7E+07	19.19
24	645276	933888	3.7E+07	3.7E+07	19.62
24	645186	934098	3.7E+07	3.7E+07	20.19
25	647586	931538	6.7E+06	6.8E+06	16.08
25	647676	931748	6.8E+06	6.9E+06	15.73
25	647586	931948	6.9E+06	7.0E+06	16.58
25	647586	932178	7.0E+06	7.0E+06	18.78
	Villa Camilla anticline				⟷
25	647616	932418	7.0E+06	7.0E+06	19.41
25	647656	932648	7.0E+06	7.3E+06	17.94
25	647806	932808	7.3E+06	7.3E+06	16.22
25	647876	932948	7.3E+06	7.4E+06	14.29
25	647966	933158	7.4E+06	7.4E+06	13.08
25	647896	933368	7.4E+06	7.6E+06	12.84
25	647956	933598	7.6E+06	7.6E+06	13.18
25	647996	933828	7.6E+06	7.6E+06	13.70
25	647946	934048	7.6E+06	8.0E+06	14.75
25	647966	934288	8.0E+06	8.0E+06	16.62
25	648036	934508	8.0E+06	8.2E+06	18.22
	Castelvetro anticline				⟷
25	648176	934698	8.2E+06	8.2E+06	17.73
25	648106	934928	8.3E+06	8.3E+06	16.20
25	647976	935128	8.3E+06	8.5E+06	15.00
25	647876	935308	8.5E+06	8.7E+06	13.59
25	647746	935468	8.7E+06	1.1E+07	13.08
26	648686	931138	1.1E+06	1.1E+06	13.30
26	648656	931368	1.1E+06	1.2E+06	14.09
26	648636	931608	1.2E+06	1.4E+06	13.68
26	648516	931808	1.4E+06	2.4E+06	12.48
	Villa Camilla anticline				⟷
26	648536	931988	2.4E+06	2.5E+06	10.38
26	648466	932178	2.5E+06	2.5E+06	9.35
26	648516	932378	2.5E+06	2.6E+06	9.10
26	648456	932598	2.6E+06	3.0E+06	8.92
26	648536	932818	3.0E+06	3.1E+06	8.58
26	648586	933048	3.1E+06	3.2E+06	8.52
26	648636	933278	3.2E+06	4.6E+06	9.06
26	648706	933498	4.6E+06	4.7E+06	9.39
26	648786	933718	4.7E+06	5.0E+06	9.27
26	648736	933938	5.0E+06	5.0E+06	9.16
	Castelvetro anticline				⟷
26	648846	934138	5.0E+06	5.1E+06	9.12
26	649016	934278	5.1E+06	5.2E+06	9.10
26	649196	934408	5.2E+06	5.3E+06	9.04
26	649366	934538	5.3E+06	5.6E+06	9.02
26	649486	934718	5.6E+06	5.6E+06	9.11
26	649496	934958	5.6E+06	6.0E+06	9.28
27	649466	930608	4.3E+07	4.3E+07	34.02
27	649626	930778	4.3E+07	4.4E+07	33.69
27	649816	930928	4.4E+07	4.4E+07	33.41
27	650006	931078	4.4E+07	4.5E+07	33.02
27	650156	931208	4.5E+07	4.5E+07	32.25
	Villa Camilla anticline				⟷
27	650316	931368	4.5E+07	4.5E+07	31.71
27	650356	931608	4.5E+07	4.5E+07	31.31
27	650466	931788	4.5E+07	4.5E+07	30.90
27	650646	931938	4.5E+07	4.5E+07	30.63
27	650866	932018	4.5E+07	4.5E+07	30.22
27	651086	932098	4.5E+07	4.6E+07	29.32
27	651166	932258	4.6E+07	4.6E+07	28.42

Table 3 (*continued*)

Stream	Easting[a]	Northing[a]	Min_area[b]	Max_area[b]	k_{sn}[c]
27	651126	932498	4.6E+07	4.7E+07	27.62
	Castelvetro anticline				⟷
27	651156	932698	4.7E+07	4.7E+07	27.27
27	651126	932908	4.7E+07	4.7E+07	28.26
27	651136	933138	4.7E+07	4.7E+07	30.68
27	651326	933268	4.7E+07	4.8E+07	32.44
27	651436	933458	4.8E+07	4.8E+07	32.42
27	651526	933668	4.8E+07	4.8E+07	30.90
27	651706	933808	4.8E+07	4.8E+07	29.15
28	651466	929828	3.1E+06	3.2E+06	22.25
28	651666	929928	3.2E+06	7.0E+06	20.56
28	651896	929998	7.0E+06	7.2E+06	18.67
28	652096	930128	7.2E+06	7.2E+06	16.95
	Villa Camilla anticline				⟷
28	652306	930148	7.2E+06	8.7E+06	15.91
28	652476	930228	8.7E+06	8.9E+06	16.12
28	652676	930328	8.9E+06	1.1E+07	17.59
28	652806	930438	1.1E+07	1.1E+07	18.68
28	652846	930668	1.1E+07	1.2E+07	19.67
28	652876	930898	1.2E+07	1.2E+07	20.06
28	652876	931118	1.2E+07	1.2E+07	19.66
28	652996	931278	1.2E+07	1.3E+07	19.18
28	653106	931478	1.3E+07	1.3E+07	18.42
28	653206	931688	1.3E+07	1.3E+07	17.37
28	653366	931828	1.3E+07	1.3E+07	16.41
	Castelvetro anticline				⟷
28	653506	932008	1.3E+07	1.5E+07	15.96
28	653686	932118	1.5E+07	1.5E+07	15.65
28	653916	932148	1.5E+07	1.6E+07	15.24
28	654106	932308	1.6E+07	1.6E+07	14.85
28	654296	932408	1.6E+07	1.7E+07	14.54
29	651196	930918	2.3E+04	8.1E+04	8.31
29	651366	931058	8.7E+04	1.3E+05	9.27
29	651516	931228	1.3E+05	1.5E+05	8.28
29	651436	931448	1.5E+05	3.1E+05	7.77
29	651556	931638	3.1E+05	4.3E+05	6.50
29	651686	931818	4.3E+05	5.1E+05	6.29
29	651906	931888	5.1E+05	1.1E+06	7.06
29	652096	932008	1.1E+06	1.1E+06	6.96
29	652286	932168	1.1E+06	1.5E+06	7.20
	Villa Camilla anticline				⟷
29	652356	932388	1.5E+06	1.7E+06	7.82
29	652486	932578	1.7E+06	2.0E+06	8.55
29	652706	932648	2.0E+06	2.1E+06	9.22
29	652806	932838	2.1E+06	2.3E+06	9.26
29	653026	932918	2.3E+06	2.4E+06	9.16
30	650986	930408	6.3E+05	9.0E+05	9.62
30	651186	930428	9.2E+05	1.1E+06	11.70
30	651396	930408	1.1E+06	1.2E+06	12.89
30	651606	930478	1.2E+06	1.3E+06	12.65
30	651806	930608	1.3E+06	1.4E+06	11.74
	Villa Camilla anticline				⟷
30	651986	930768	1.4E+06	1.4E+06	10.98
30	652146	930948	1.4E+06	1.6E+06	10.15
30	652276	931148	1.6E+06	1.7E+06	9.57
30	652346	931368	1.7E+06	1.8E+06	9.00
30	652516	931548	1.8E+06	1.9E+06	8.31
30	652696	931688	1.9E+06	1.9E+06	8.06
30	652846	931878	2.0E+06	2.0E+06	12.01
30	653026	932058	2.0E+06	2.1E+06	15.95
	Castelvetro anticline				⟷
30	653236	932018	2.1E+06	2.1E+06	16.73
30	653466	932068	2.1E+06	2.1E+06	21.09
32	652246	927598	2.8E+04	6.0E+04	13.50
32	652296	927808	6.0E+04	2.5E+05	14.65
32	652436	928008	2.6E+05	3.5E+05	12.67
32	652496	928228	3.6E+05	5.4E+05	12.02
32	652506	928478	5.4E+05	7.0E+05	15.72
32	652536	928708	7.0E+05	8.9E+05	19.04
32	652616	928928	9.0E+05	9.8E+05	17.01
32	652776	929118	9.8E+05	1.1E+06	19.32
	Villa Camilla anticline				⟷
32	652916	929298	1.2E+06	1.3E+06	19.64
32	652976	929528	1.3E+06	1.4E+06	16.00
32	652996	929768	1.4E+06	1.6E+06	12.88
32	652966	930008	1.6E+06	1.7E+06	14.47

(*continued on next page*)

Table 3 (*continued*)

Stream	Easting[a]	Northing[a]	Min_area[b]	Max_area[b]	k_{sn}[c]
32	652816	930198	1.7E+06	2.0E+06	22.78
33	653446	927038	2.0E+07	2.0E+07	33.30
33	653656	927038	2.0E+07	2.3E+07	34.76
33	653846	927138	2.3E+07	2.3E+07	32.43
33	653996	927318	2.3E+07	2.3E+07	28.35
33	654116	927518	2.3E+07	2.3E+07	25.97
33	654166	927748	2.3E+07	2.4E+07	23.00
33	654126	927968	2.4E+07	2.4E+07	20.12
33	654246	928168	2.4E+07	2.5E+07	19.36
	Villa Camilla anticline				⟷
33	654376	928348	2.5E+07	2.5E+07	19.82
33	654496	928538	2.5E+07	2.5E+07	20.27
33	654566	928748	2.5E+07	2.6E+07	20.78
33	654616	928948	2.6E+07	2.6E+07	21.51
33	654666	929138	2.6E+07	2.6E+07	21.96
33	654666	929368	2.6E+07	2.6E+07	22.55
33	654766	929538	2.6E+07	2.7E+07	23.10
33	654796	929768	2.7E+07	2.9E+07	23.47
33	654766	929998	2.9E+07	2.9E+07	23.45
33	654886	930188	2.9E+07	3.0E+07	22.86
33	654896	930388	3.0E+07	3.0E+07	22.16
33	655016	930588	3.0E+07	3.0E+07	21.93
33	655186	930768	3.0E+07	3.0E+07	22.04
33	655296	930968	3.0E+07	3.0E+07	22.13
	Castelvetro anticline				
33	655306	931198	3.0E+07	3.1E+07	22.28
33	655446	931388	3.1E+07	3.1E+07	22.62
33	655576	931568	3.1E+07	3.1E+07	23.16
33	655726	931738	3.1E+07	3.1E+07	23.59
33	655856	931938	3.1E+07	3.2E+07	23.99
33	655916	932168	3.2E+07	3.2E+07	23.98
33	655856	932388	3.2E+07	3.2E+07	23.74
34	653006	928258	1.2E+04	1.4E+05	15.18
34	653056	928488	1.4E+05	2.7E+05	14.81
34	653186	928678	2.7E+05	3.5E+05	13.11
34	653346	928858	3.6E+05	4.3E+05	12.57
	Villa Camilla anticline				⟷
34	653536	928978	4.3E+05	8.4E+05	13.07
34	653696	929138	8.4E+05	9.3E+05	12.13
34	653866	929308	9.3E+05	9.6E+05	11.12
34	653906	929538	9.6E+05	1.0E+06	11.08
34	653916	929778	1.0E+06	1.4E+06	11.71
34	654056	929938	1.4E+06	1.8E+06	12.26
34	654296	929948	1.8E+06	2.1E+06	12.76
34	654506	929918	2.1E+06	2.1E+06	19.35
34	654716	929928	2.1E+06	2.1E+06	33.12
38	654736	926458	4.1E+05	5.4E+05	14.19
38	654886	926638	5.4E+05	6.4E+05	15.28
38	655076	926788	6.4E+05	8.7E+05	14.23
38	655196	926958	8.8E+05	9.8E+05	13.49
38	655266	927178	9.8E+05	1.8E+06	11.76
38	655456	927328	1.8E+06	1.9E+06	8.31
38	Villa Camilla anticline				⟷
38	655606	927518	1.9E+06	2.0E+06	11.15
38	655786	927698	2.0E+06	2.0E+06	18.03
38	655986	927798	2.0E+06	2.4E+06	19.76
38	656196	927708	2.4E+06	2.5E+06	15.77
38	656376	927868	2.5E+06	2.6E+06	14.62
38	656566	928018	2.6E+06	3.3E+06	16.84
38	656736	928148	3.3E+06	3.7E+06	17.26
38	656956	928198	3.7E+06	3.8E+06	15.37
38	657786	928448	4.2E+06	4.3E+06	10.89
38	657986	928478	4.3E+06	4.4E+06	10.65
38	658146	928628	4.4E+06	7.5E+06	12.00
38	658336	928778	7.6E+06	7.6E+06	13.32
38	658496	928958	7.7E+06	7.7E+06	13.49
38	658686	929098	7.7E+06	7.8E+06	13.62
38	658866	929278	7.8E+06	7.9E+06	13.63
	Castelvetro anticline				⟷
38	659026	929428	7.9E+06	8.0E+06	13.65
38	659106	929648	8.0E+06	8.1E+06	13.67
38	659136	929888	8.1E+06	8.1E+06	13.48
38	659196	930108	8.1E+06	8.4E+06	13.21
38	659316	930308	8.4E+06	8.5E+06	13.03
38	659256	930538	8.5E+06	8.5E+06	12.81
38	659226	930768	8.5E+06	8.8E+06	12.77

Table 3 (*continued*)

Stream	Easting[a]	Northing[a]	Min_area[b]	Max_area[b]	k_{sn}[c]
36	655846	929138	6.1E+05	7.8E+05	7.38
36	655986	929338	7.8E+05	9.0E+05	8.94
36	656086	929548	9.1E+05	1.0E+06	10.16
36	656136	929778	1.0E+06	1.2E+06	10.31
36	656206	929988	1.2E+06	1.3E+06	10.46
36	656246	930218	1.3E+06	1.6E+06	10.87
36	656256	930458	1.6E+06	1.6E+06	11.02
36	Castelvetro anticline			⟷	
36	656256	930708	1.6E+06	2.0E+06	10.93
36	656256	930938	2.0E+06	2.2E+06	10.63
36	656236	931178	2.2E+06	2.3E+06	10.36
36	656246	931418	2.3E+06	2.4E+06	10.34
36	656346	931618	2.4E+06	2.6E+06	10.34
36	656456	931828	2.6E+06	2.6E+06	10.30
36	656556	932018	2.6E+06	2.7E+06	10.42
36	656756	932058	2.7E+06	2.7E+06	11.22
37	656226	928578	2.8E+05	4.6E+05	6.41
37	656366	928768	4.6E+05	5.9E+05	7.73
37	656496	928968	6.0E+05	7.1E+05	9.33
37	656676	929118	7.1E+05	8.3E+05	10.34
37	656876	929258	8.3E+05	9.1E+05	10.29
37	657106	929298	9.1E+05	9.5E+05	9.74
37	657316	929388	9.5E+05	1.4E+06	9.30
37	Villa Camilla anticline				⟷
37	657396	929598	1.4E+06	1.8E+06	9.05
37	657556	929758	1.8E+06	1.8E+06	9.08
37	657656	929958	1.8E+06	2.6E+06	8.62
37	657826	930148	2.7E+06	2.7E+06	9.05
37	657836	930388	2.7E+06	2.8E+06	12.56
37	657916	930588	2.8E+06	3.0E+06	15.49
37	658116	930698	3.0E+06	3.3E+06	15.27
37	658216	930888	3.3E+06	3.3E+06	14.34
39	655806	926338	4.4E+04	1.4E+05	19.78
39	656016	926438	1.4E+05	2.3E+05	19.82
39	656156	926618	2.3E+05	3.5E+05	16.76
39	656256	926828	3.5E+05	4.4E+05	15.62
	Villa Camilla anticline				⟷
39	656346	927038	4.4E+05	5.2E+05	19.38
39	656506	927228	5.4E+05	6.4E+05	19.43
39	656636	927418	6.4E+05	6.8E+05	15.86
39	656846	927518	6.8E+05	7.7E+05	13.88
39	657056	927598	7.9E+05	8.1E+05	14.38
39	657286	927608	8.1E+05	1.3E+06	15.24
39	657476	927618	1.3E+06	2.1E+06	13.71
39	657626	927788	2.1E+06	2.2E+06	11.33
39	657766	927938	2.2E+06	2.5E+06	10.31
39	657876	928108	2.7E+06	2.8E+06	9.86
40	656876	926538	3.7E+04	1.4E+05	14.62
40	657096	926528	1.4E+05	2.1E+05	10.44
40	657316	926548	2.1E+05	2.5E+05	10.98
	Villa Camilla anticline				⟷
40	657456	926738	2.5E+05	3.4E+05	15.33
40	657486	926958	3.4E+05	4.2E+05	15.91
40	657516	927198	4.2E+05	5.1E+05	12.55
40	657546	927408	5.1E+05	7.0E+05	12.74
40	657546	927638	7.0E+05	7.0E+05	13.55
41	660196	926768	8.5E+07	8.5E+07	36.38
41	660436	926788	8.5E+07	8.6E+07	40.55
41	660646	926898	8.6E+07	9.0E+07	40.31
41	660846	927008	9.0E+07	9.6E+07	38.80
41	661086	927038	9.6E+07	9.6E+07	37.13
41	661246	927218	9.6E+07	9.6E+07	34.50
41	661386	927408	9.6E+07	9.6E+07	32.41
	Villa Camilla anticline				⟷
41	661396	927658	9.6E+07	9.7E+07	30.41
41	661466	927878	9.7E+07	9.7E+07	27.53
41	661586	928078	9.7E+07	9.7E+07	23.05
41	661636	928308	9.7E+07	9.8E+07	18.79
41	661756	928508	9.8E+07	9.8E+07	18.29
41	661806	928738	9.8E+07	9.8E+07	18.95
41	661956	928928	9.8E+07	1.0E+08	19.67

[a] Spatial reference of data Projection: European Datum 1950 Transverse Mercator, fuse 32N.

[b] Drainage area expressed in m^2. Read 2.7E + 07 as 2.7×10^7.

[c] Calculated with $\theta_{ref} = 0.45$.

may indicate a lower threshold for the tectonic forcing that can be recorded in channel profiles.

We note that the swath profile incorporates (Fig. 6) the axial lines (vertical dashed lines in Fig. 6) of both the Castelvetro and the Villa Camilla anticlines (Fig. 2). Long-term slow growth of these structures at about 0.2 mm/year is supported by topographic dissection of the uplifted Po Plain and smooth graded profiles of the subenvelope. There are no obvious knickpoints in the valleys. Similarly, the Castelvetro anticlinal hinge shows a spike in the profile (see km 9.1 in Fig. 7A) that coincides with the mapped location of an active NE–SW oriented reverse fault in the subsurface (Ponza, 2010, Ph.D. dissertation).

In contrast, the swath profile across the Ghiardo plateau (Fig. 8A) shows little topographic dissection and the envelopes closely parallel the fold structure consistent with recent growth. We suggest that this morphology stems two factors (Burbank and Vergés, 1994): (i) the formation of a young topography that, despite the decreasing uplift rates of the anticlines to 0.18 mm/year in the last 450–620 ka (see Section 4.1), is probably related to a contemporary decrease in background subsidence of the foreland (Ponza, 2010, Ph.D. dissertation); and (ii) the response to erosion and the development of a limited drainage network into the high permeable Middle Pleistocene conglomerates being deformed atop of the Ghiardo plateau.

The spatial distribution of k_{sn} values in the Ghiardo Plateau overlaps with the general topographic and structural evidence for growing anticlines. Here k_{sn} maxima and minima coincide with the frontal limb and synclinal hinge respectively of the anticline, a pattern well expressed by stream 13 in Fig. 8A. Given the general lack of stream incision across this anticline, it appears that the greatest degrees of channel steepness changes are focused in the zones of greatest structural tilt. These observations are particularly true for small channels with an upstream drainage area <20 km^2 (e.g., streams 1, 3, 10, 11, 13; Table 2). One interpretation of this distinction in the k_{sn} response in small verses large streams is that the larger streams, sourced in the high Apennines are transport-limited, influenced by orographic precipitation, and have all of the attendant variations in the erosion coefficient (K) that have been demonstrated to influence k_{sn} (Snyder et al., 2000). Therefore, if the interpretation is correct, our analysis selects those parts of the channel that are most reflective of detachment-limited fluvial processes and avoids the upper reaches dominated by debris flows and the lower segments that have become alluvial and transport-limited.

Channel steepness corresponds differently for the Villa Camilla anticline with respect to the Ghiardo Plateau (Figs. 11 and 12). For Villa Camilla anticline the smoothed k_{sn} maxima coincide with the fold hinge area (Fig. 12) and also locally with the greatest relief (Fig. 6). Along strike, there is a general correspondence between high relief and high k_{sn} values (Figs. 7A, B), but the pattern is complicated by regions of high k_{sn} and little fluvial dissection (relief). For example, some of the highest k_{sn} values for small streams traversing the Villa Camilla anticline correspond with the along-strike transition from the gently uplifted tip to the more strongly uplifted core, a transition that occurs at about km 8 in Fig. 7B. As the anticline grows, the zone of greatest limb rotation and plunge move outward from the core to the tips with the high k_{sn} values, indicating the location of a recently tilted area that has yet to be incised by the transverse streams. This is consistent with our interpretation for the distribution of the high k_{sn} values in the Ghiardo Plateau as falling on those parts of the anticline currently undergoing the strongest tilting without the commensurate response of fluvial incision.

Dependence of k_{sn} values on uplift rate have been explored in several recent studies (e.g., Snyder et al., 2000, Kirby and Whipple, 2001, Wobus et al., 2006, Kirby et al., 2007) with the main conclusion being that k_{sn} generally scales linearly with uplift rate, if the erosion constant K truly remains constant. We use local relief as a proxy for rock uplift across the mountain front and anticlines. We are justified in doing this because the topographic envelope parallels middle Pleistocene stratigraphic markers preserved in the landscape. Pleistocene incision has been into a former low-relief surface that has been uplifted as a plateau and gently deformed. This plateau-like character is very evident for the Ghiardo area (Figs. 3 and 8A), less so for the Castelvetro area (Fig. 2), but in both cases the stratigraphic markers are preserved. Similar to most studies, we assume that river incision across the anticlines is being driven primarily by rock uplift so the production of relief in the transverse valleys should scale with incision rate (uplift rate).

In our study, the long-term rates of anticline growth are similar among the three areas and do not provide a sufficient explanation for the variable distribution or range of k_{sn} values. Rather, we appeal to the degree of topographic dissection (relief), the relative age of the structures, and the propagation of transient parts of the channel (knickpoints) through the fluvial system as a better explanation for the k_{sn} data.

Our assumption that relief is a justifiable measure of uplift rate is not supported by the k_{sn} and topographic data (Fig. 13). In setting

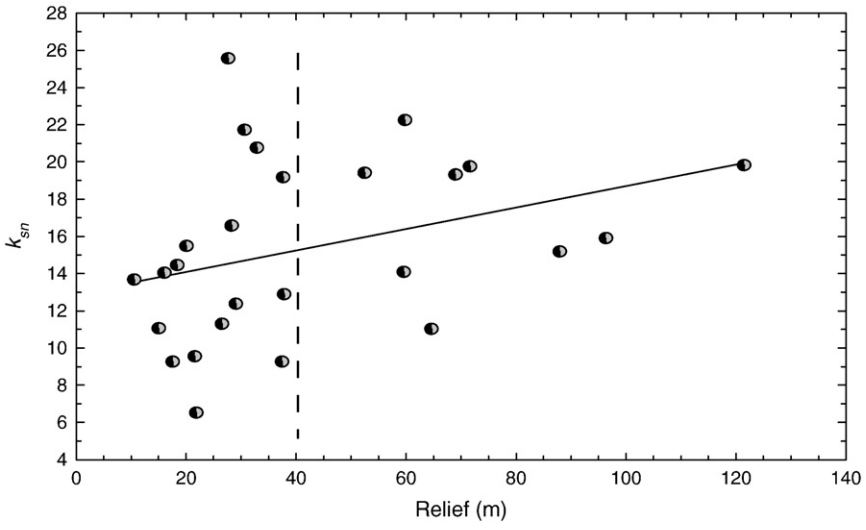

Fig. 13. Relationship between maximum k_{sn} values and their relative relief including data representative of all the three investigated structures. The dashed line separates regions with greater than 40 m generated relief, from regions where low-uplift rates have created relief <40 m.

with rapid rock-uplift rates, relief grows rapidly and reaches a steady state with fluvial incision and basin denudation. Here, we would predict a relationship between k_{sn} and relief because both would rapidly reach steady-state values reflecting the tectonic forcing. But in our low rock-uplift setting, we suspect that there are significant lags times in the response of the fluvial system to the tectonic forcing, responses that can be further influenced by sedimentologic and hydrologic influences on K. As a result, k_{sn} and relief have not achieved steady-state values and we appeal to transient responses to the tectonic forcing. For example, the regular trend of the maximum k_{sn} values located some hundreds of meters from the Ghiardo anticline hinge, together with the less-developed drainage network on the plateau (see swath profile of Fig. 8A), indicate that the growth of the Ghiardo anticline is comparatively more recent and that the small transverse ephemeral streams are in a transient state of incision with respect to the growing topography where the k_{sn} maximum values may represent knickpoints migrating upstream toward the plateau bulge.

In general, the spatial distribution of k_{sn} values appears to coincide with fold uplift and deformation, as indicated by the location of the fold axes (Fig. 12), tilting towards the foreland (Fig. 11), or tilting along strike as a growing fold propagates laterally (Fig. 7B). However, there is no compelling or consistent relationship between k_{sn} and relief (Fig. 13). We favor an interpretation where, in this slowly deforming landscape, there is a lag time between the tectonic forcing and fluvial response of incision that generates the relief. In this case, the high k_{sn} values indicate places where the channels are being actively deformed by tectonics, but have not yet fully responded by incising and generating relief. For low-uplift rate settings where <40 m of relief have been created, k_{sn} appears to be completely insensitive to the deformation (Fig. 13). For regions with greater than 40 m of relief, the tectonic forcing may be strong enough to create a weak dependence of k_{sn} on relief and uplift rate (Fig. 13).

6. Conclusions

In summary, our results are not consistent with other studies that have argued for a linear scaling relationship between the rate of rock uplift, measured as river incision, and k_{sn} values, if we use relief as a proxy for those uplift rates. Our results show that a weak linear scaling between rock uplift and k_{sn} may hold for our highest uplift settings where over 40 m of relief have been generated, thus establishing a lower threshold for where the channel steepness approach may be valid. It is interesting to point out that the k_{sn} values can be explained in terms of tectonic forcing at geologic time and space scales even if that forcing is not directly or easily reflected in the generation of topographic relief. For example, Snyder et al. (2000) report a general k_{sn} dependency on rock uplift, influenced by a non-constant K, where the rock-uplift rate varies from 1 to 4 mm/year. Similarly, the Kirby and Whipple (2001) study reports k_{sn} variations across anticlinal uplift rates spanning nearly an order of magnitude. We conclude that for the small streams traversing the Po Plain anticlines, K may be constant, or nearly constant, allowing variation in k_{sn} to be driven by rock uplift. Otherwise, we would expect to see no correspondence between relief and k_{sn}, even at the scale of an individual growing structure (Fig. 8A).

Our analysis however also decidedly resolves the matter of continued shortening in the Apennine foreland. Slow deformation throughout the Pleistocene is clearly supported from the deformation of middle Pleistocene lithostratigraphic markers, including fluvial terraces, but there has been lingering uncertainty in the contemporary growth of the structures. The good correspondence among the stratigraphic markers used to define the structures, topography and relief as quantified in the swath profiles presented here, and the k_{sn} values that indicate active channel adjustments to tectonic forcing collectively support continued shortening across the European–Adria plate boundary and growth of the Apennines.

References

Amorosi, A., Caporale, L., Cibin, U., Colalongo, M.L., Pasini, G., Ricci Lucchi, F., Severi, P., Vaiani, S.C., 1998. The Pleistocene littoral deposits (Imola Sands) of the northern Apennines piedmont. Giornale di Geologia 60, 83–118.

Balestrieri, M.L., Bernet, M., Brandon, M.T., Picotti, V., Reiners, P., Zattin, M., 2003. Pliocene and Pleistocene exhumation and uplift of two key areas of the northern Apennines. In: Bartolini, C., Piccini, L., Catto, N.R. (Eds.), Uplift and Erosion; Driving Processes and Resulting Landforms; Dynamic Relations Between Crustal and Surficial Processes: Quaternary International, 101–102, pp. 67–73.

Bally, A.W., Burbi, L., Cooper, C., Ghelardoni, R., 1986. Balanced sections and seismic reflection profiles across the central Apennines. Memorie della Societài Geologica Italia 35, 257–310.

Bartolini, C., 2003. When did the Northern Apennine become a mountain chain? In: Bartolini, C., Piccini, L., Catto, N.R. (Eds.), Uplift and Erosion; Driving Processes and Resulting Landforms; Dynamic Relations Between Crustal and Surficial Processes: Quaternary International, 101–102, pp. 75–80.

Bernini M., Papani, G., 1987. Alcune considerazioni sulla struttura del margine appenninico emiliano fra il T. Stirone ed il T. Enza (e sue relazioni con il Sistema del Taro). Atti Meeting "Brittle deformation analysis in neotectonics", Firenze, 17 aprile 1986, L'Ateneo Parmense.

Blythe, A.E., Burbank, D.W., Farley, K.A., Fielding, E.J., 2000. Structural and topographic evolution of the central Transverse Ranges, California, from apatite fission-track, (U–Th)/He and digital elevation model analyses. Basin Research 12, 97–114. doi.10.1046/j.1365-2117.2000.00116.x.

Boccaletti, M., Coli, M., Eva, C., Ferrari, G., Giglia, G., Lazzarotto, A., Merlanti, A., Nicolich, F., Papani, R., Postpischl, G., 1985. Considerations on the seismotectonics of the northern Apennines. Tectonophysics 117, 7–38.

Boccaletti, M., Bonini, M., Corti, G., Gasperini, P., Martelli, L., Piccardi, L.,Tanini, C., Vannucci, G., 2004. Seismotectonic Map of the Emilia-Romagna Region, 1:250000. Regione Emilia- Romagna CNR. SELCA, Firenze, Italy

Burbank, D., Vergés, J., 1994. Reconstruction of topography and related depositional systems during active thrusting. Journal of Geophysical Reseach 99, 20,281–20,297.

Carnicelli, S., Caporale, L., Marchi, N., Iasio, C., Ferrari, G.A., Guermandi, M., Tarocco, P., 2003. Paleosoils of the Margin, a Case of Study in the Reggio-Emilia Province; Notes for Field Excursion. Pre-Congress Field Trip, 4th Cartography European Congress, Bologna, Italy. http://www.regione.emilia-romagna.it/wcm/geologia/canali/convegni_e_seminari/congresso_europeo/congresso_04/Pre_Congress_Field_Trip.pdf.

Cremaschi, M., Papani, G., 1975. Contributo preliminare alla neotettonica del margine padano dell'appennino: le forme terrazzate comprese tra Cavriago e Quattro Castella (Reggio E.). Acta Naturalia de l'Ateneo-Parmense 11, 335–371.

Duvall, A., Kirby, E., Burbank, D., 2004. Tectonic and lithologic controls on bedrock channel profiles in coastal California. Journal of Geophysical Reseach 109, F03002. doi.10.1029/2003JF000086.

Elter, P., Giglia, G., Tongiorgi, M., Trevisan, L., 1975. Tensional and compressional areas in the recent (Tortonian to present) evolution of the Northern Apennines. Bollettino Geofisica Teorica e Applicata 17, 3–8.

Eppes, M.C., Bierma, R., Vinson, D., Pazzaglia, F.J., 2008. A soil chronosequence study of the Reno valley, Italy: insights into the relative role of climate versus anthropogenic forcing on hillslope processes during the mid-Holocene. Geoderma 147 (3–4), 97–107.

Finnegan, N.J., Roe, G., Montgomery, D.R., Hallet, B., 2005. Controls on the channel width of rivers: implications for modeling of fluvial incision of bedrock. Geology 33, 229–232.

Flint, J.J., 1974. Stream gradient as a function of order, magnitude and discharge. Water Resources Research 10, 969–973.

Gasperi, G., Bettelli, G., Panini, F., Pizziolo, M., 1999. Note illustrative alla Carta Geologica d' Italia a scala 1:50000 Foglio n 219 Sassuolo. Servizio Geologico d'Italia.

Hack, J.T., 1957. Studies of Longitudinal Profiles in Virginia and Maryland. U. S. Geological Survey Professional Paper 294-B, pp. 45–97.

Harkins, N., Kirby, E., Eimsath, A., Robinson, R., Reiser, U., 2007. Transient fluvial incision in the headwaters of the Yellow River, northeastern Tibet, China. Journal of Geophysical Research 112. doi.10.1029/2006JF000570.

Hill, K., Hayward, A., 1988. Structural constraints on the Tertiary plate tectonic evolution of Italy. Marine and Petroleum Geology 5, 2–6.

Isacks, B.L., 1992. Long term land surface processes: erosion, tectonics and climate history in mountain belts. In: Mather, P.M. (Ed.), TERRA-1: Understanding the Terrestrial Environment. Taylor and Francis, London, pp. 21–36.

Kirby, E., Whipple, K.X., 2001. Quantifying differential rock-uplift rates via stream profile analysis. Geology 29, 415–418.

Kirby, E., Johnson, C.B., Furlong, K.P., Heimsath, A., 2007. Transient channel incision along Bolinas Ridge, California: evidence for differential rock uplift, adjacent to the San Andreas fault. Journal of Geophysical Reseach 112 (F03S07).

Lavecchia, G., Boncio, P., Creati, N., 2003. A lithospheric-scale seismogenic thrust in central Italy. Journal of Geodynamics 36, 79–94.

Lavecchia, G., Boncio, P., Creati, N., Brozzetti, F., 2004. Stile strutturale, stato termo-meccanico e significato sismogenetico del thrust Adriatico; dati e spunti da una revisione del profilo CROP 03 integrata con l'analisi di dati sismologici. Bollettino della Società Geologics Italiana 123, 111–125.

Masek, J.G., Isacks, B.L., Gubbels, T.L., Fielding, E.J., 1994. Erosion and tectonics at the margins of continental plateaus. Journal of Geophysical Research 99 (B7), 941–956.

Merritts, D.J., 1996. The Mendocino triple junction: active faults, episodic coastal emergence, and rapid uplift. Journal of Geophysical Research 101, 6051–6070. doi.10.1029/95JB01816.

Merritts, D.J., Bull, W.B., 1989. Interpreting Quaternary uplift rates at the Mendocino triple junction, northern California, from uplifted marine terraces. Geology 17, 1020–1024.

Molin, P., Pazzaglia, F.J., Dramis, F., 2004. Geomorphic expression of active tectonics in a rapidly-deforming forearc, Sila Massif, Calabria, southern Italy. American Journal of Science 304, 559–589.

Picotti, V., Pazzaglia, F.J., 2008. A new active tectonic model for the construction of the Northern Apennines mountain front near Bologna (Italy). Journal of Geophysical Research 113 (B8), 1–24.

Picotti, V., Capozzi, R., Bertozzi, G., Mosca, F., Sitta, A., Tornaghi, M., 2007. The Miocene petroleum system of the Northern Apennines in the central Po Plain (Italy). In: Lacombe, O., Rome, F. (Eds.), Thrust Belts and Foreland Basins, From Fold Kinematics to Hydrocarbon System. Springer Verlag, Berlin, pp. 117–131.

Ponza, A., 2010. Tectonic geomorphology and active strain of the Northern Apennines mountain front. PhD dissertation, University of Bologna.

Roe, G.H., Montgomery, D.R., Hallet, B., 2002. Effects of orographic precipitation variations on the concavity of steady-state river profiles. Geology 30, 143–146.

Royden, L., 1993. Evolution of retreating subduction boundaries formed during continental collision. Tectonics 12, 629–638.

Scrocca, D., 2006. Thrust front segmentation induced by differential slab retreat in the Apennines (Italy). Terra Nova 18, 154–161.

Scrocca, D., Carminati, E., Doglioni, C., Marcantoni, D., 2007. Slab retreat and active shortening along the Central-Northern Apennines. In: Lacombe, O., Roure, F. (Eds.), Thrust Belts and Foreland Basins, From Fold Kinematics to Hydrocarbon System. Springer Verlag, Berlin, pp. 471–487.

Sklar, L., Dietrich, W.E., 2001. Sediment and rock strength controls on river incision into bedrock. Geology 29, 1087–1090.

Sklar, L.S., Dietrich, W.E., 2004. A mechanistic model for river incision into bedrock by saltating bed load. Water Resources Research 40, W06301. doi.10.1029/2003WR002496.

Snyder, N., Whipple, K., Tucker, G., Merritts, D., 2000. Landscape response to tectonic forcing: DEM analysis of stream profiles in the Mendocino triple junction region, northern California. Geological Society of America Bulletin 112, 1250–1263.

Snyder, N.P., Whipple, K.X., Tucker, G.E., Merrits, D.J., 2003. Channel response to tectonic forcing: field analysis of stream morphology and hydrology in the Mendocino triple junction region, northern California. Geomorphology 53, 97–127. doi.10.1016/S0169-555X(02)00349-5.

Spagnolo, M., Pazzaglia, F.J., 2005. Testing the geological influences on the evolution of river profiles: a case from the Northern Apennines (Italy). Geografia Fisica e Dinamica Quaternaria 28, 103–113.

Wegmann, K.W., Pazzaglia, F.J., 2009. Late Quaternary fluvial terraces of the Romagna and Marche Apennines, Italy: climatic, lithologic, and tectonic controls on terrace genesis in an active orogen. Quaternary Science Reviews 28 (1–2), 137–165. doi.10.1016/j.quascirev.2008.10.006.

Whipple, K.X., Tucker, G.E., 1999. Dynamics of the stream-power river incision model: implications for height limits of mountain ranges, landscape response timescales, and research needs. Journal of Geophysical Research 104, 17,661–17,674.

Whipple, K.X., Wobus, C., Krosby, B., Kirby, E., Sheehan, D., 2007. New Tools for Quantitative Geomorphology: Extraction and Interpretation of Stream Profiles from Digital Topographic Data. GSA Short Course: #506.

Wilson, L.F., Pazzaglia, F.J., Anastasio, D.J., 2009. A fluvial record of active fault-propagation folding, Salsomaggiore anticline, northern Apennines, Italy. Journal of Geophysical Reseach 114 (B8). doi.10.1029/2008JB005984.

Wobus, C., Whipple, K.X., Kirby, E., Snyder, N., Johnson, J., Spyropolou, K., Crosby, B., Sheehan, D., 2006. Tectonics from topography: procedures, promise, and pitfalls. Geological Society of America Special Paper 398, 55w–74w.

Zaprowski, B.J., Evenson, E.B., Pazzaglia, F.J., Epstein, J., 2001. Knickzone propagation in the Black Hills and northern High Plains; a different perspective on the late Cenozoic exhumation of the Laramide Rocky Mountains. Geology 29 (6), 547–550.